Nuclear structure of ^{159}Gd

C. Granja* and S. Pospíšil
Institute of Experimental and Applied Physics, Czech Technical University in Prague, CZ–12800 Prague 2, Czech Republic

A. Aprahamian
Department of Physics, Notre Dame University, South Bend, Indiana 46556, USA

H. Börner and H. Lehmann
Institut Laue–Langevin, BP 156, F–38042 Grenoble, France

T. von Egidy and H.–F. Wirth
Physik–Department, Technische Universität München, D–85748 Garching, Germany

G. Graw, R. Hertenberger, and Y. Eisermann
Sektion Physik, Ludwig–Maximilians–Universität München, D–85748 Garching, Germany

D. Nosek
Faculty of Mathematics and Physics, Charles University, CZ–18000 Prague 8, Czech Republic

L. Rubáček†
Faculty of Nuclear Sciences and Physical Engineering, Czech Technical University in Prague, CZ–11519 Prague 1, Czech Republic

S. A. Telezhnikov
Joint Institute for Nuclear Research, 141–980 Dubna, M.R. Russia

(Received 23 September 2003; revised manuscript received 15 April 2004; published 30 September 2004)

The well deformed atomic nucleus ^{159}Gd was investigated by means of radiative neutron capture and single neutron transfer reactions. Nearly 70 secondary γ rays from the (n,γ) reaction studied with high-resultion bent-crystal spectrometers at Grenoble are assigned to ^{159}Gd. About 200 levels with spin up to $\frac{11}{2}$ are observed in this nucleus below 2.3 MeV in (d,p) and $(\mathbf{d},t)$ reactions investigated at the Tandem Van de Graaff accelerator in Garching using unpolarized (18 MeV) and polarized (22 MeV) deuteron beams, respectively. The proposed level scheme for this nucleus is arranged into 21 rotational bands. Experimentally observed levels are interpreted using predictions obtained within the quasiparticle-phonon model and the quasiparticle-rotor approach for a well deformed nucleus.

DOI: 10.1103/PhysRevC.70.034316 PACS number(s): 21.10.−k, 21.60.−n, 25.40.−h

I. INTRODUCTION

The experimental study of odd deformed nuclei provides the opportunity to acquire an extensive set of data for investigating various nuclear excitation modes and their interplay. In this paper, we report on results of (n,γ), (d,p), and (d,t) reactions obtained with precise spectrometers that yield detailed level scheme of the ^{159}Gd nucleus with spectroscopic information on the excited states and their decay.

Previous studies of ^{159}Gd include the transfer reactions (d,p) [1], (d,t) [1–3], (t,p) [4], and (n,α) [5,6]. Primary γ rays following neutron capture were investigated with thermal neutrons [7]. A tentative measurement with resonance neutrons was announced in Ref. [8] with merely a list of primary γ-ray energies available in Ref. [9]. Information on low-energy γ rays in this nucleus existed only from β^--decay studies of ^{159}Eu [10]. Recently, the ^{158}Gd$(n,\gamma)^{159}$Gd reaction was studied with epithermal neutrons in isolate resonance capture [11] and average resonance capture [12] yielding information on primary γ rays and levels up to 3 MeV. A set of 15 low-energy γ rays was observed in the (n,γ) reaction at isolated resonances. Most of these γ rays were placed as secondary transitions among low-lying levels [13].

Many single quasiparticle states have been identified in the level scheme of this nucleus, namely at low excitation energies [1]. However, discrepancies remain in the identification of rotational bands [1,9] and the γ decay of low-lying levels [10]. States with significant quasiparticle-vibrational components have not yet been identified in this nucleus. A number of states of quasiparticle excitations coupled with β and γ phonons have been reported in neighboring odd-A nuclei such as ^{161}Dy [14] and ^{155}Gd [15]. The level structure of these nuclei has been extensively studied experimentally, namely ^{155}Gd [15], ^{157}Gd [16], and ^{161}Dy [14]. The systematics of odd-A rare earth nuclei in this region have been reviewed in Refs. [17] and [18].

*Electronic address: carlos.granja@utef.cvut.cz
†Present address: Phys. Dept. Giessen University, Germany.

 ©2004 The American Physical Society

Attempts to describe the structure of ^{159}Gd were done using the collective model. An axially symmetric deformed Saxon-Woods potential coupled to a rotating core [19] was applied. Configuration mixing between single particle states in single nucleon transfer reactions was examined within the Nilsson model in a Saxon-Woods potential with quadrupole and hexadecapole deformation [20]. A calculation of single-particle wave functions, form factors and level energies in a deformed Saxon-Woods potential was applied to the ^{160}Gd$(d,t)^{159}$Gd reaction [21]. The experimental angular dependence of the differential cross sections of this reaction, that could not be satisfactorily described by the distorted wave born approximation (DWBA) and the anomalous spectroscopic factors (relative to Nilsson model predictions), were investigated in terms of multistep processes, vibrational admixtures and Coriolis coupling [22]. Calculations within the coupled channels born approximation (CCBA) were insufficient to explain these discrepancies [23,24]. Recently, the pseudo $SU(3)$ shell model has been used to describe negative-parity bands in the neighboring nuclei ^{157}Gd and ^{159,163}Dy [25–27].

This paper is devoted to the spectroscopic information obtained from the investigation of ^{159}Gd with (n,γ), (d,p), and $(\mathbf{d},t)$ reactions. We aim at elucidating the structure of excited bands in particular and the systematics for deformed nuclei of this region in general [15,18,28,29]. Model calculations are provided in this work in order to interprete the spectroscopic results obtained.

The setup, collection, and evaluation of spectroscopic results of the experimental investigations are given in the next section. The level and decay schemes which are constructed exclusively from the experimental results are given in Sec. III. The structure of ^{159}Gd interpreted in terms of rotational bands is presented in Sec. IV. The energy systematics of quasiparticle states between adjacent odd-A nuclei is summarized in Sec. V. In Sec. VI, we report on results of the Coriolis band mixing calculations based upon the intrinsic structure given by the quasiparticle-phonon model (QPM). This model was used to interpret the experimental data, propose configuration assignments for the observed levels and improve the knowledge about the structure of this nucleus. Conclusions are given in Sec. VII.

II. EXPERIMENTS AND SPECTROSCOPIC RESULTS

A. The ^{158}Gd$(n,\gamma)^{159}$Gd reaction

Low-energy γ rays in ^{159}Gd were measured with the high resolution bent-crystal spectrometers GAMS2/3 [30] at the high flux reactor in the Institut Laue-Langevin, Grenoble. The target consisted of 55 mg Gd_2O_3 enriched in ^{158}Gd to 98.0% wrapped in aluminum foil. The stringent requirements on energy resolution [30] required a very thin target of dimensions $55\times4\times0.07$ mm. Traces of neighboring isotopes with large cross sections, namely ^{155}Gd and ^{157}Gd (6.1×10^4 and 2.5×10^5 b, respectively [31]) were burned up in-pile in the high flux of thermal neutrons 5×10^{14} cm^{-2} s^{-1} for about 3 and 1 days, respectively. The thermal neutron cross section of ^{158}Gd is merely 2.2 b [31]. Gamma-ray spectra were collected with time steps of 60 s in the range from 150 keV to 1.5 MeV controlling the rotation of the bent crystals by means of a laser interferometer [32].

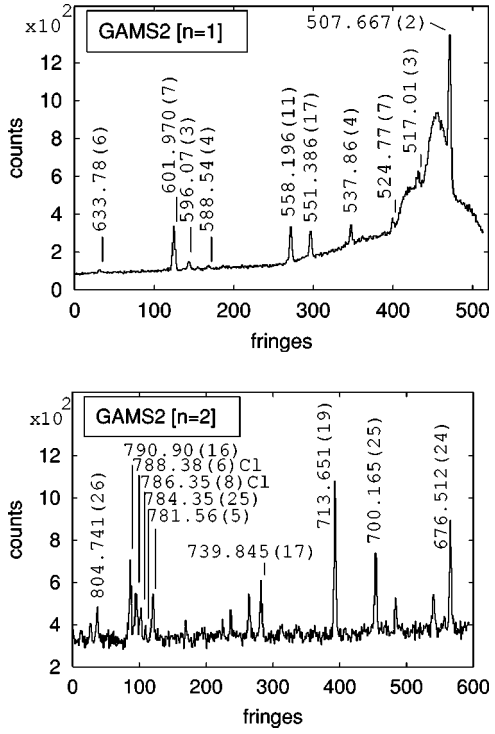

FIG. 1. Parts of γ-ray spectra recorded with the GAMS2 spectrometer. Some peaks are labeled with their energy in kilo-electronvolts. Background peaks are indicated (chlorine).

Figure 1 shows parts of γ-ray spectra recorded with the GAMS2 spectrometer in first and second order of Bragg diffraction. The broad profile in the upper spectrum results from source geometry of annihilation quanta arising in the target sample, foil, and holder. The energy resolution was $\Delta E_\gamma(\mathrm{keV}) = 2.5\times10^{-6}[E_\gamma(\mathrm{keV})]^2/n$ where n is the order of reflection [30]. Gamma rays in ^{156}Gd, with energies precisely known from a previous experiment [33] with the ultrahigh resolution double-flat-crystal spectrometer GAMS4 [34], were used for calibration. The 626.322 keV transition in ^{156}Gd [33] was used as the main calibration reference. Gamma-ray spectra were converted from interference fringes to gamma-ray energies by means of an interferometric function [30,32].

Peaks in the spectra were fitted with the code GASPAN of Rieß [35]. The intensities of the γ rays were corrected for self-absorption in the target and internal conversion. Their values were then normalized to the number of neutrons captured using the 601.969 keV transition in ^{159}Gd, previously determined in neutron capture at isolated resonances [13]. Background lines included γ rays from Al and Cl (see Fig. 1). Several γ rays previously assigned to ^{249}Cm in the reaction ^{248}Cm$(n,\gamma)^{249}$Cm [36] were observed in our experiment. These γ rays, namely the 831.35, 941.48, 982.90, and 1013.59 keV lines, are properly assigned to neutron capture in ^{27}Al [37].

A total of 67 secondary γ rays in ^{159}Gd are presented in Table I. About half of these γ rays are observed for the first

TABLE I. Secondary γ rays observed in the reaction ^{158}Gd(n,γ) ^{159}Gd with the GAMS2/3 spectrometers. The placement in the proposed level scheme is included.

E_γ(keV)	$I_\gamma(\gamma_s/100\ n)$[a]	E_i(keV)$\rightarrow E_i$(keV)[b]
95.685(5)	2.6(4)	146.316$\rightarrow$50.627
138.996(6)	0.46(10)	
146.324(7)[c]	1.44(17)	146.316$\rightarrow$0.0
159.547(10)[c]	0.34(7)	227.412$\rightarrow$67.829
172.368(15)	0.27(6)	818.089$\rightarrow$646.697
181.84(9)	0.39(6)	
184.163(7)	0.41(7)	330.479$\rightarrow$146.316
273.856(21)	0.17(8)	781.556$\rightarrow$507.724
313.851(8)	0.23(3)	915.828$\rightarrow$601.977
326.873(18)	0.15(3)	
358.264(28)	0.17(2)	1139.84$\rightarrow$781.556
364.029(20)	0.26(3)	1145.60$\rightarrow$781.556
416.09(5)	0.23(4)	974.29$\rightarrow$558.211
466.618(11)[d,e]	1.43(14)	588.517$\rightarrow$121.899
		974.29$\rightarrow$507.724
507.639(20)[e,f]	3.68(27)	558.211$\rightarrow$50.624
507.727(20)[e,f]	5.2(4)	507.724$\rightarrow$0.0
524.77(7)[e]	0.95(8)	646.697$\rightarrow$121.899
534.12(6)	0.28(4)	601.977$\rightarrow$67.829
537.86(4)[e]	1.38(15)	588.517$\rightarrow$50.627
551.385(17)[c,e]	2.08(11)	601.977$\rightarrow$50.627
558.195(11)[e]	2.67(26)	558.211$\rightarrow$0.0
581.71(9)	0.11(3)	1139.84$\rightarrow$558.211
582.85(6)	0.23(3)	633.60$\rightarrow$50.627
588.54(4)[c,d]	0.23(5)	588.517$\rightarrow$0.0
		710.38$\rightarrow$121.899
596.066(24)[c]	0.79(3)	646.697$\rightarrow$50.627
601.969(7)[c,e]	4.30(14)	601.977$\rightarrow$0.0
633.78(6)	0.36(4)	633.60$\rightarrow$0.0
646.75(9)[c,e]	1.33(9)	646.697$\rightarrow$0.0
659.26(8)[c]	0.29(4)	710.38$\rightarrow$50.627
665.04(5)[c]	0.20(3)	732.87$\rightarrow$67.829
676.512(24)[c,e]	1.71(8)	744.378$\rightarrow$67.829
678.53(6)	0.25(4)	800.45$\rightarrow$121.899
681.71(6)[e]	0.73(5)	800.45$\rightarrow$118.686
693.73(6)[c]	0.49(6)	744.378$\rightarrow$50.627
700.163(25)[e]	1.00(19)	818.89$\rightarrow$118.686
713.649(19)[e]	2.0(4)	781.556$\rightarrow$67.829
726.47(8)[c]	0.12(2)	872.64$\rightarrow$146.316
732.68(8)[c]	0.15(4)	800.45$\rightarrow$67.829
739.843(17)[c]	0.74(12)	858.51$\rightarrow$118.686
744.375(20)[c,e]	0.60(14)	744.378$\rightarrow$0.0
751.23(5)	0.48(4)	818.89$\rightarrow$67.829
754.03(9)[c]	0.29(5)	872.64$\rightarrow$118.686
768.15(6)	0.28(3)	818.89$\rightarrow$50.627
781.56(5)	0.97(6)	781.556$\rightarrow$0.0
784.35(25)	0.20(3)	
790.90(16)	1.52(19)	858.51$\rightarrow$67.829
800.39(14)	0.23(4)	800.45$\rightarrow$0.0
804.739(26)[c]	0.73(4)	872.64$\rightarrow$67.829
807.60(11)	0.43(4)	858.51$\rightarrow$50.627
813.12(4)	0.15(7)	880.63$\rightarrow$67.829
834.85(14)	0.23(4)	
858.39(5)	0.75(17)	858.51$\rightarrow$0.0
933.08(6)[d]	1.21(27)	1159.90$\rightarrow$227.412
		1079.39$\rightarrow$146.316
951.06(29)	0.29(9)	1001.62$\rightarrow$50.627
963.85(10)	1.20(11)	1110.25$\rightarrow$146.316
974.72(6)	0.45(28)	974.29$\rightarrow$0.0
1000.51(11)	0.82(11)	
1001.61(19)	0.66(10)	1001.62$\rightarrow$0.0
1015.02(14)[c]	0.65(8)	
1028.62(11)	1.13(9)	1079.39$\rightarrow$50.627
1061.63(11)[c]	1.64(9)	1061.70$\rightarrow$0.0
1078.57(8)[c]	1.00(15)	1128.73$\rightarrow$50.627
1082.37(15)	0.49(8)	1134.7$\rightarrow$50.627
1095.18(8)[c]	0.84(14)	1145.60$\rightarrow$50.627
1121.4(5)	0.45(9)	
1128.47(17)[c]	1.16(6)	1128.73$\rightarrow$0.0
1139.90(8)	1.93(15)	1139.84$\rightarrow$0.0

[a]Transition intensities (given per 100 captured neutrons) are corrected for target self-absorption.
[b]Values derived from LeFit calculations (see Sec. III).
[c]Observed also in β^- decay of ^{159}Eu [10].
[d]Unresolved doubles.
[e]Observed also at isolated neutron resonance capture [13].
[f]Doublet identified in Ref. [13] and resolved with GAMS4.

time; a third of the 60 γ rays previously reported in β^- decay [10] are observed in our data. All 15 secondary γ rays previously observed at isolated neutron resonances [13] are confirmed. The peak at 507.668 keV (see Fig. 1), previously identified as a doublet by analyzing correlations between primary and secondary γ rays at isolated resonance neutron capture [13], was resolved in a parallel test run of the double-flat-crystal spectrometer GAMS4 (see Table I).

B. The ^{158}Gd$(d,p)^{159}$Gd reaction

The (d,p) reaction was studied with an unpolarized 18 MeV deuteron beam at the Munich Tandem accelerator [38]. The target consisted of a 130-μg cm^{-2}-thick layer of Gd_2O_3 (enriched in ^{158}Gd to 97.0%) evaporated on a 5.6-μg cm^{-2}-thick carbon foil. The reaction products were analyzed with the Q3D magnetic spectrograph [39] and detected in its 1.8 m long focal plane. A long position sensitive detector consisting of two single wire proportional chambers, a multiwire proportional chamber and a plastic scintillator with $\Delta E/E_{\rm rest}$ particle identification for background suppression

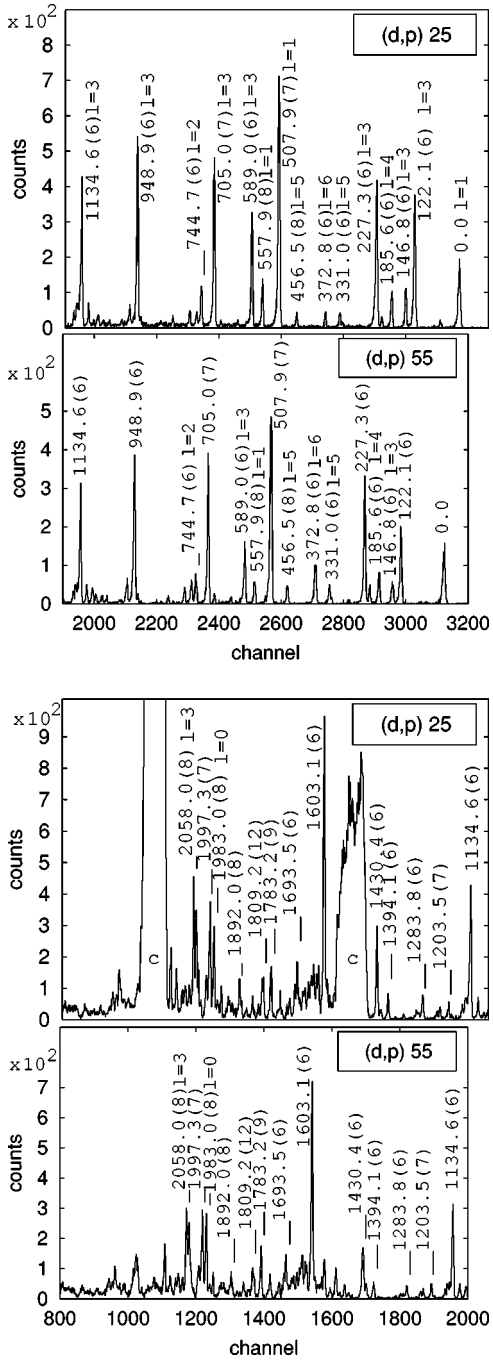

FIG. 2. Proton spectra in the ^{158}Gd$(d,p)^{159}$Gd reaction at 25° and 55° with 18 MeV deuterons. Some peaks are labeled by the corresponding level energy (in kilo-electron-volts). Note that the peaks for the levels are marked with the transferred angular momenta *l*. Background contributions of light elements in the target (marked as c) appear broadened and exhibit a different position (kinematic shift) at different angles.

was used [40]. A Faraday cup behind the target integrated the beam current. We recorded spectra at angles $\theta_{\rm lab}=13^\circ$, 17°, 21°, 25°, 30°, 35°, 40°, 45°, and 55°.

Parts of proton spectra measured at 25° and 55° are presented in Fig. 2. The energy range recorded corresponded to levels up to 3.5 MeV in ^{159}Gd with overall resolution of full width at half maximum (FWHM) $\approx$5 keV. A systematic error of the long position sensitive detector was estimated at 0.5 keV. Particle identification was possible via a two-dimensional plot of the energy loss in the proportional chamber versus the energy deposition in the scintillator. The energy calibration made use of the well-established level energies in ^{159}Gd deduced from the precise measurement of low-energy γ rays in the (n,γ) reaction (see Table I).

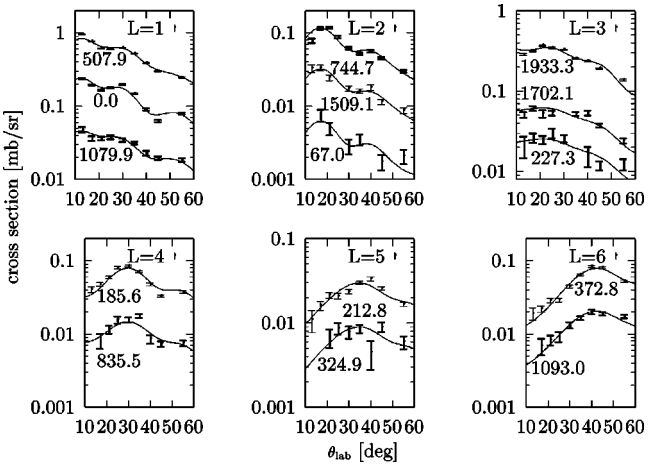

FIG. 3. Differential cross sections for the ^{158}Gd$(d,p)^{159}$Gd reaction at 18 MeV. Level energies (in kilo-electron-volts) and tranferred angular momenta (in $\hbar$) are indicated.

Thus, well established reference levels were available up to about 1.2 MeV. Above this energy, peaks were gradually identified with new levels obtained by the Ritz combination principle using the (n,γ) data. These levels were used in turn to calibrate the (d,p) spectra in an iterative procedure up to 2 MeV. Above this energy, an unambiguous identification of peaks was increasingly difficult due to the high level density. The fitting procedure of proton spectra was done with the program GASPAN of Rieß [35].

The differential cross sections for several levels in ^{159}Gd with different transferred angular momenta *l* are shown in Fig. 3. Predictions based on DWBA are included (see Sec. II E). From the analysis of the differential cross sections, the tranferred angular momentum *l* can be determined for a given level. Consequently, the total angular momentum is derived as $j=l\pm\frac{1}{2}$. The parity of the level is given by $\pi=(-1)^l$. The differential cross sections for all measured levels are given in Ref. [41] together with the detailed description of their analysis.

C. The ^{160}Gd$(d,t)^{159}$Gd reaction

The $(\mathbf{d},t)$ reaction was measured with the Q3D magnetic spectrograph [39] at the Munich Tandem accelerator [38] with a polarized 22 MeV deuteron beam. The target consisted of a 125-μg cm^{-2}-thick layer of Gd_2O_3 (enriched in ^{160}Gd to 98.2%) evaporated on a 14-μg cm^{-2}-thick carbon backing. This reaction was measured with a vector polarized beam at angles $\theta_{\rm lab}=12^\circ$, 16°, 20°, 25°, 30°, and 35° using the Munich Stern-Gerlach ion source [42]. The angular distribution was measured for levels above 650 keV. This experiment made use of a new (but shorter) cathode strip detector

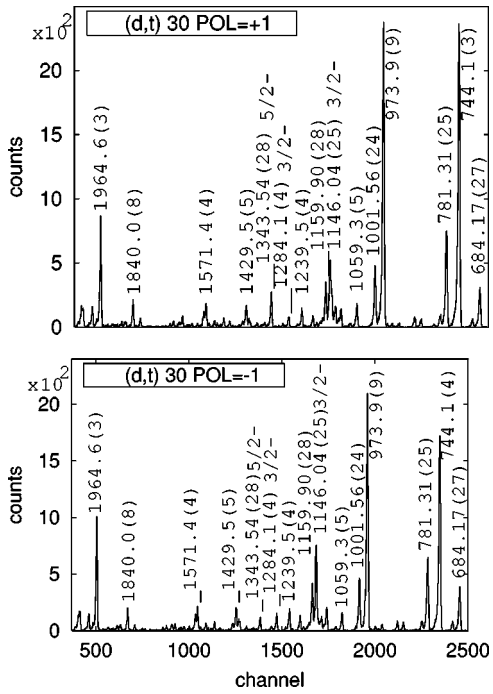

FIG. 4. Parts of triton spectra at 30° in the ^{160}Gd($\mathbf{d},t$)^{159}Gd reaction with spin up (+1) and down (−1) polarized deuterons at 22 MeV. Note the relative peak sizes of indicated $3/2^-$ and $5/2^-$ levels. Some peaks are labeled by the correponding level energy (in kilo-electron-volts).

with single strip readout [43,44] which is able to handle higher beam currents (>1 μA). Overall energy resolution was FWHM $\approx$7 keV. The systematic error of the cathode strip detector was estimated at 0.2 keV.

Parts of triton spectra recorded at 30° are shown in Fig. 4. Peaks in the spectra were fitted with the code GASPAN of Rieß [35]. The experimental analyzing power is determined from the relation

$$A_y = \frac{2}{3P_y}\frac{\sigma_+ - \sigma_-}{\sigma_+ + \sigma_-}, \tag{1}$$

where σ_+ and σ_- are the measured differential cross sections with respect to the polarization of the beam. The vector polarization (along the direction transverse to the beam) was P_y=70(10)% [45]. The effect of using a polarized beam can be seen in the triton spectra shown in Fig. 4 for the $3/2^-$ and $5/2^-$ levels.

The energy calibration at low excitation energy used well established levels in ^{159}Gd which are precisely determined from the accurately measured secondary γ rays in our (n,γ) experiment (see Table I). Additionally, we compared the measurements of the ^{126}Te(d,t)^{125}Te and ^{160}Gd(d,t)^{159}Gd reactions under the same conditions. Both reactions were measured in a separate short run at 20° with equal settings of the Q3D spectrograph magnets. According to the kinematical shift, the ground state of ^{125}Te was seen in the ^{159}Gd spectrum as an excited level at 1670 keV. Few excited levels in ^{125}Te were correspondingly observed at higher energies and

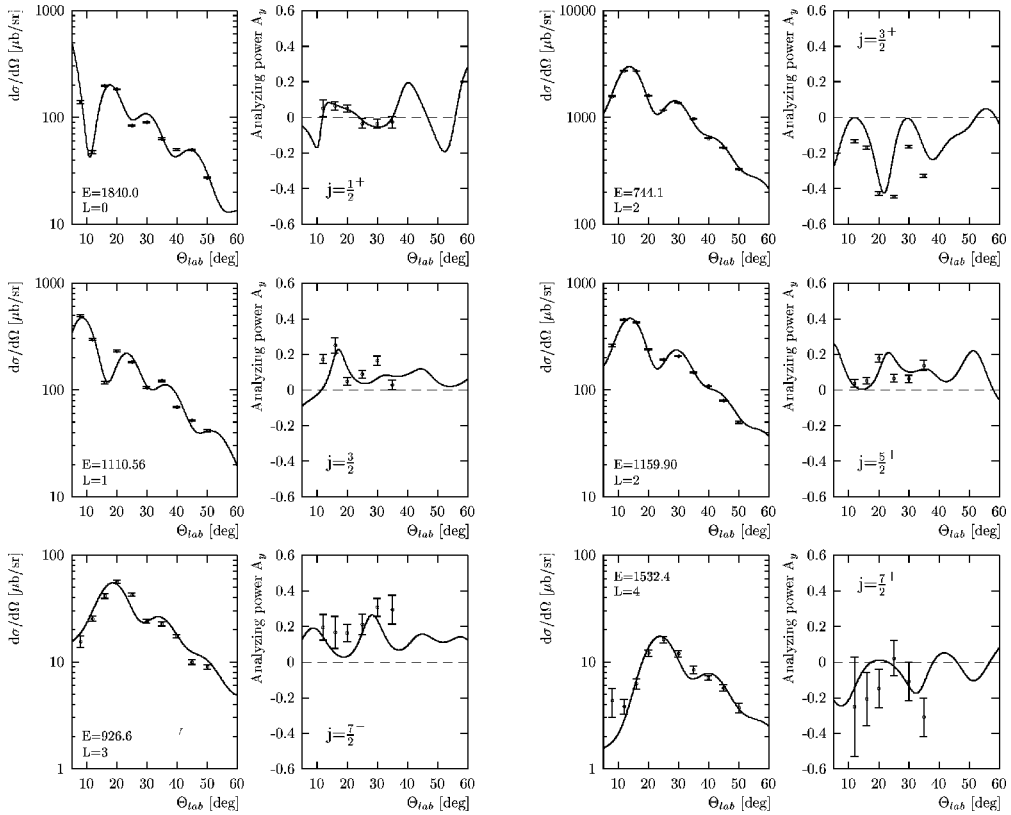

FIG. 5. Differential cross sections and analyzing powers of the ^{160}Gd($\mathbf{d},t$)^{159}Gd reaction at E_d=22 MeV. DWBA calculations are included as solid lines. Level energies (in kilo-electron-volts) and transferred and total angular momenta (in $\hbar$) are given.

served mainly as a control of polynomial extrapolation beyond the last calibration point (at 1841 keV) up to 2.3 MeV.

The differential cross sections for several levels populated in ^{159}Gd with different transferred angular momenta l are depicted in Fig. 5. Predictions based on DWBA are included (see Sec. II E). For a given level, the transferred angular momentum l is determined from the analysis of angular dependence of the differential cross section. From the analysis of the angular distribution of the analyzing power, the total angular momentum j is unambiguously determined.

D. The ^{160}Gd$(d,t)^{159}$Gd reaction

The single neutron pickup reaction was also investigated with an unpolarized 25 MeV deuteron beam at angles $\theta_{\rm lab}$ $=8^{\circ}$, 40°, 45°, and 50° using a similar sample, beam energy and the "short" focal plane detector [43] as the $(\mathbf{d},t)$ experiment with a polarized beam described in Sec. II C. In a separate run, this reaction was studied at 20° with the "long" focal plane detector [40] used in the (d,p) experiments. Parts of the triton spectrum recorded in this measurement are shown in Fig. 6.

E. DWBA analysis

The differential cross sections and analyzing powers (see Figs. 3 and 5) were interpreted in terms of the distorted wave born approximation. Calculations were performed with the computer program CHUCK3 of Kunz [46]. Parameters of the optical potentials for deuterons, protons and tritons were taken from Refs. [47], [48], and [49], respectively. The values corresponding to our experimental settings are listed in Table II. A sample of the input files for the CHUCK3 calculations is included in Ref. [41]. For a given incident particle energy, transferred and total angular momenta, and shell model n_{lj} configuration for each level, CHUCK3 generates the corresponding differential cross section and analyzing power.

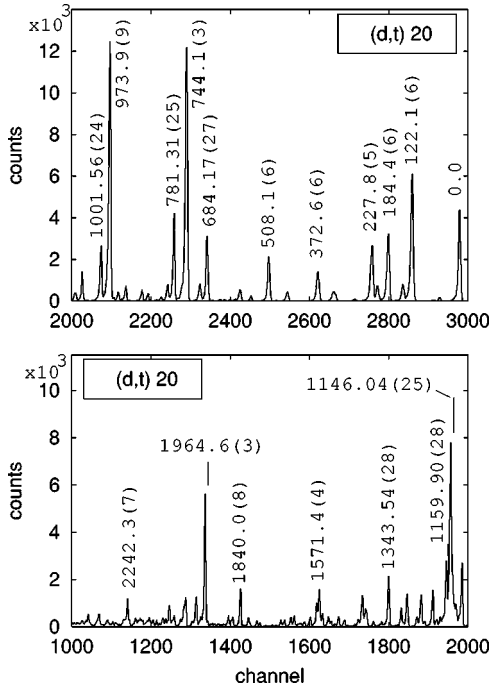

FIG. 6. Parts of triton spectrum at 20° in the ^{160}Gd$(d,t)^{159}$Gd reaction with 25 MeV unpolarized deuterons. Some peaks are labeled by the corresponding level energy (in kilo-electron-volts).

The spectroscopic factor S_{lj} for the stripping (d,p) reaction, and the spectroscopic strength G_{lj} for the pickup (d,t) reaction, result from the measured and calculated differential cross sections as

$$\frac{d\sigma^{\rm exp}}{d\Omega} = S_{lj}\sigma_{lj}^{\rm CHUCK3}\cdots({\rm d,p}), \tag{2}$$

$$\frac{d\sigma^{\rm exp}}{d\Omega} = G_{lj}\sigma_{lj}^{\rm CHUCK3}\cdots({\rm d,t}). \tag{3}$$

The spectroscopic factor is related to the spectroscopic strength by $G_{lj}=(2j+1)S_{lj}$. The shape and peak maxima position of the differential cross section are determined by the value of the transferred angular momentum l. Using a polarized beam, the slight dependence on the total angular momentum j can be distinguished by means of the analyzing power, see Eq. (1).

For few levels, the angular dependence of the differential cross section in the (d,p) experiment could not be satisfactorily fitted with DWBA. Some of these cases are indicated in Fig. 7 where the nearest–l DWBA fits are shown. Levels with the irregular differential cross section are indicated in Table III. Below 1.2 MeV, these levels are namely 51.2, 557.9, 684.1, 874.5, 938.6, and 1151.0 keV. We tentatively attempted to describe these irregular cross sections in terms of the coupled channels born approximation. Preliminary calculations were performed [41] with the code CHUCK3 [46]. The cases were considered where a vibrational phonon of the even-even core couples to a single quasiparticle state of the unpaired neutron in the deformed field. The lowest vibrations

TABLE II. Optical parameters used in DWBA.

		^{158}Gd$(d,p)^{159}$Gd			^{160}Gd$(d,t)^{159}$Gd		
		d	p	n	d	t	n
V_r	(MeV)	94.24	56.45	[a]	118.64	140.61	[a]
$4W_D$	(MeV)	49.46	34.46		50.29		
W_0	(MeV)					20.80	
V_{so}	(MeV)	6.81	12.40	$\lambda=25$	7.30	9.50	$\lambda=25$
r_r	(fm)	1.17	1.22	1.25	1.15	1.16	1.25
r_D	(fm)	1.33	1.32		1.29		
r_0	(fm)					1.20	
r_{so}	(fm)	1.07	1.01		0.88	1.10	
R_c	(fm)	1.30	1.25		1.30	1.40	
a_r	(fm)	0.74	0.75	0.75	0.88	0.75	0.75
a_D	(fm)	0.91	0.64		0.89		0.65
α_0	(fm)					0.82	
a_{so}	(fm)	0.66	0.75		1.00	0.80	
nlc		0.54	0.85	0.85	0.54	0.30	0.85

[a]Adjusted by CHUCK3.

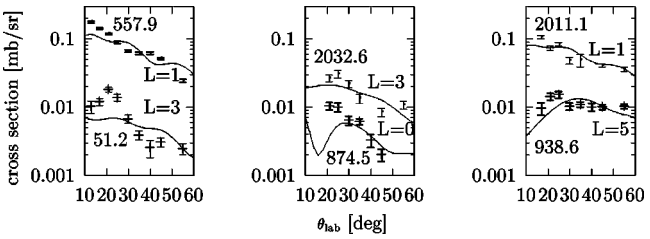

FIG. 7. Differential cross sections of the ^{158}Gd$(d,t)^{159}$Gd reaction with irregular DWBA fit. Level energy (in kilo-electron-volts) and transferred angular momenta are shown.

in the adjacent even-even nuclei ^{158}Gd and ^{160}Gd were taken into account, namely the 1^- and γ vibrations at 977 and 988 keV, respectively [50]. However, no significant improvement over the DWBA approach was obtained. This confirmed that the applicability of CCBA to describe the ^{160}Gd$(d,t)^{159}$Gd reaction [22,23] is limited.

F. Levels from the transfer reactions

About 200 levels observed in the stripping and pickup reaction experiments in ^{159}Gd are presented in Table III. The analysis of the differential cross sections [and the analyzing powers in the $(\mathbf{d},t)$ reaction] resulted in assignments of transferred and total angular momenta for most levels. In the cases where the asymmetries in the analyzing powers of $(\mathbf{d},t)$ cross sections could not be unambiguously determined, the two possible values of spin are proposed. Due to the lack of reference lines in the calibration above 2.1 and 2.3 MeV in the (d,p) and $(\mathbf{d},t)$ reactions, respectively, we present results only up to the indicated energies in the following.

III. LEVEL AND DECAY SCHEME

A. The level scheme

The proposed level scheme is based on the following experimental information: (i) the levels identified in the (d,p) and $(\mathbf{d},t)$ reactions presented in Table III; (ii) the secondary γ rays observed in radiative neutron capture and their placement among low-lying levels (see Table I); and (iii) the nearly 180 levels populated by primary γ rays from our previous (n,γ) experiments at isolate [11] and average [12] neutron resonance capture.

A total of 276 levels in the ^{159}Gd nucleus observed in the (n,γ), (d,p) and $(\mathbf{d},t)$ reactions are listed in Table IV. Final level energies (column 1) are obtained as weighted averages of the energies derived in the transfer reaction experiments (column 3) and the energies deduced from the primary γ-ray experiments [11,12] (column 5). Precise values of energies for most levels below 1.2 MeV were obtained thanks to the placement of the secondary γ rays accurately measured. The proposed values result from a χ^2 fit between the observed transitions and the proposed levels using the code LEFIT of Schreckenbach [51]. In all other cases, the weighted averages of the experimental results are given. Final assignments of level spins and parities (column 2) result from the combination of spectroscopic results (columns 4 and 6) and from the construction of rotational bands (see Sec. IV). The selectivity of the $(\mathbf{d},t)$ reaction helped to make many definite assignments on level spin and parity values.

B. Levels from previous publications

Among 19 levels reported in the β^- decay of ^{159}Eu [10], 18 levels are confirmed in our data; we do not observe the high-lying level at 1351.8 keV. All levels reported in the previous (d,p) experiment [1] are confirmed up to 1.1 MeV while at higher energies, 14 levels are not observed. Below 1 MeV, we observe in our (d,p) data new levels at 51.2, 67.0, 212.8, 324.9, 601.8, 632.9, 819.5, 858.4, and 938.6 keV. All levels reported in the previous (d,t) experiment with unpolarized deuterons (within ±5 keV) [1] are confirmed. The previously observed level at 327 keV [1] appears in our $(\mathbf{d},t)$ experiments as a resolved doublet with $\frac{11}{2}^-$ at 324.9 keV and $\frac{9}{2}^-$ at 330.8 keV. Newly observed levels in our $(\mathbf{d},t)$ experiment lying below 1 MeV also include the levels at 602.2, 633.4, 646.5, and 876.6 keV.

C. Decay scheme

The investigation of the depopulation of low-lying levels is based on the low-energy γ rays observed in thermal neutron capture listed in Table I and in β^- decay of ^{159}Eu [10]. The γ-decay scheme proposed for many levels below 1.2 MeV is presented in Table V. Several transitions reported in the β^- decay of ^{159}Eu [10], which could be placed among these levels, are included.

IV. STRUCTURE OF ^{159}GD

A. Configuration assignments

Whereas level energies, spins, and parities are determined by the combined experimental spectroscopic information, the configuration assignments of levels are, to some extent, model dependent. To this end, model predictions are used to identify the levels observed in the experiments. The identification of intrinsic configurations and their associated rotational bands are in this work based on Nilsson model and are guided by (i) experimental systematics of band head energies [17,18] presented in Sec. V and our empirical band parameters listed in Table VI; (ii) Nilsson schemes provided by our calculations and by other authors, see Refs. [18 and 50]; (iii) the level energies and spectroscopic factors observed in the (d,p) and $(\mathbf{d},t)$ experiments and their comparison with model predictions described in Sec. VI and summarized in Tables VIII and IX; and (iv) the observed decay of low-lying levels which should be similar for members of the same band leading to related bands. We also made use of the the information provided by the low-energy γ rays reported in the β^- decay of the ^{159}Eu nucleus [10] compiled in Table V together with our (n,γ) results. Note that the spectroscopic factors given in Table IX for the $(\mathbf{d},t)$ reaction for levels lying below 650 keV, the values of which we used in the interpretation, were deduced [assuming the same J^π values of the (d,p) reaction] from only one measurement (at angle 20°) with an unpolarized beam.

TABLE III. Spectroscopic information for ^{159}Gd from (d,p) and $(\mathbf{d},t)$ reactions. The level energies and spin-parity values deduced are given along with the cross section (at $\theta_{lab}=30°$) and the corresponding spectroscopic factor or spectroscopic strength [see Eqs. (2) and (3)]. Uncertain assignments are given in parenthesis.

(d,p)				$(\mathbf{d},t)$			
E_x(keV)[a]	$d\sigma/d\Omega(\mu b/sr)$[b]	J^π	$S_{jl}(10^{-3})$[c]	E_x(keV)[d]	$d\sigma/d\Omega(\mu b/sr)$[b]	J^π	$G_{jl}(10^{-3})$
0.0	197	$1/2^-,3/2^-$	62	0.0[h]	511[h]		66[h,i]
51.2(9)	7	$(5/2^-,7/2^-)$[e]	(3)	51.0(8)[h]	22[h]		8[h,i]
67.0(7)	3	$3/2^+,5/2^+$	2	66.2(9)[h]	6[h]		3[h,i]
				119.2(9)[h]	63[h]		91[h,j]
122.1(6)	242	$5/2^-,7/2^-$	91	122.1(6)[h]	672[h]		184[h,i]
146.8(6)	71	$5/2^-,7/2^-$	27	145.4(6)[h]	106[h]		36[h,i]
185.6(6)	85	$7/2^+,9/2^+$	118	184.4(6)[h]	307[h]		90[h,i]
212.8(6)	24	$9/2^-,11/2^-$	70	212.3(6)[h]	55[h]		177[h,i]
227.3(6)	328	$5/2^-,7/2^-$	121	227.8(5)[h]	252[h]		66[h,i]
274.0(7)	4	$11/2^+,13/2^+$	27	273.7(9)[h]	6[h]		61[h,i]
324.9(8)	8	$9/2^-,11/2^-$	40	324.9(6)[h]	18[h]		33[h,i]
331.0(6)	35	$9/2^-,11/2^-$	70	330.6(8)[h]	22[h]		71[h,i]
372.8(6)	44	$11/2^+,13/2^+$	373	372.6(6)[h]	121[h]		756[h,i]
456.5(8)	28	$9/2^-,11/2^-$	78	456.4(6)[h]	26[h]		47[h,i]
507.9(7)	626	$1/2^-,3/2^-$	219	508.1(6)[h]	251[h]		30[h,i]
557.9(8)	66	$(1/2^-,3/2^-)$[e]	(58)	558.2(10)[h]	23[h]		2[h,i]
589.0(6)	182	$5/2^-,7/2^-$	67	588.6(7)[h]	63[h]		59[h,i]
601.8(12)	1	$3/2^+,5/2^+$	3	602.2(13)[h]	9[h]		4[h,i]
632.9(10)	10	$7/2^+,9/2^+$	12	633.4(7)[h]	4[h]		5[h,i]
				646.5(10)[h]	7[h]		3[h,i]
684.1(7)	12	$(9/2^-,11/2^-)$[e]	(32)	684.1(27)	188	$(11/2^-)$[e]	(978)
705.0(7)	332	$(5/2^-,7/2^-)$	(110)	705.3(4)	42	$7/2^-$	117
744.7(6)	61	$3/2^+,5/2^+$[f]	31	744.1(3)	1367	$3/2^+$	920
759.8(8)	29	$9/2^-,11/2^-$	(74)				
781.6(6)	38	$1/2^+$	12	781.3(25)	454	$1/2^+$	126
				800.4(6)	50	$3/2^+,5/2^+$	36
				819.4(7)	10	$3/2^+,5/2^+$	15
819.5(8)	1	$11/2^+,13/2^+$	7				
835.5(8)	16	$(7/2^+,9/2^+)$	(5)				
858.4(8)	4	$3/2^+,5/2^+$	2	858.8(6)	39	$3/2^+$	27
874.5(11)	6	$(1/2^+)$[e]	(4)				
876.0(9)[h]	5[h]		3[g]	876.6(5)	47	$(7/2^+,9/2^+)$[e]	(163)
926.8(7)[h]	3[h]		3[g]	926.6(4)	24	$7/2^-$	662
938.6(8)	10	$(9/2^-,11/2^-)$[e]	(29)	938.7(7)	12[h]		11[h,i]
948.9(6)	360	$5/2^-,7/2^-$	716	948.8(5)	19	$7/2^-$	47
				962.4(6)	11	$3/2^+$	7
974.4(6)	58	$1/2^+$	20	973.9(9)	1341	$1/2^+$	359
1001.2(8)	7	$3/2^+,5/2^+$	3	1001.56(24)	276	$3/2^+$	173
				1014.9(8)	3	$1/2^+$	2
1043.1(7)	12	$9/2^-,11/2^-$	26	1043.2(6)	3[h]		2[h,i]
1060.8(11)	8	$3/2^+,5/2^+$	4	1059.3(5)	101	$5/2^+$	78
1079.9(8)	24	$1/2^-,3/2^-$	8	1079.9(4)	80	$1/2^-$	37
1093.0(7)	13	$11/2^+,13/2^+$	88				
1111.5(8)	34	$1/2^-,3/2^-$	12	1110.56(27)	105	$3/2^-$	194
				1120.3(5)	23	$7/2^+$	92
				1128.8(5)	71	$3/2^+$	43

TABLE III. (*Continued.*)

(*d*,*p*)				(**d**,*t*)			
E_x(keV)[a]	$d\sigma/d\Omega(\mu b/sr)$[b]	J^π	$S_{jl}(10^{-3})$[c]	E_x(keV)[d]	$d\sigma/d\Omega(\mu b/sr)$[b]	J^π	$G_{jl}(10^{-3})$
1134.6(6)	260	$5/2^-,7/2^-$	42	1134.9(6)	25	$(7/2^-)$[e]	(52)
				1139.81(27)	95	$1/2^-$	170
1145.2(16)	21	$1/2^-,3/2^-$	8	1146.04(25)	335	$3/2^-$	615
1151.0(9)	34	$(1/2^+)$[e]	7				
1160.4(7)	28	$3/2^+,5/2^+$	13	1159.90(28)	207	$5/2^+$	108
				1170.9(4)	26	$1/2^+$	6
				1178.6(5)	16	$5/2^-$	55
				1190.5(6)	18	$5/2^+$	9
1194.2(8)	8	$7/2^+,9/2^+$	9				
				1202.6(5)	57	$9/2^+$	206
1203.5(7)	34	$9/2^-,11/2^-$	66				
				1216.9(8)	2	$1/2^-$	3
1229.8(8)	22	$7/2^+,9/2^+$	24	1229.1(6)	7	$9/2^+$	68
1239.1(9)	8	$(5/2^-,7/2^-)$	(3)	1239.5(4)	90	$(7/2^-)$[e]	(123)
				1253.1(5)	10	$5/2^-$	58
1283.8(6)	44	$(7/2^+,9/2^+)$[e]	(47)				
				1284.1(4)	58	$3/2^-$	100
1296.6(7)	6	$1/2^-,3/2^-$	2	1296.4(6)	7	$3/2^-$	9
1303.7(6)	11	$5/2^-,7/2^-$	3	1303.2(5)	16	$7/2^-$	75
				1315.8(4)	4	$1/2^+$	1
1322.2(11)	1	$(3/2^+,5/2^+)$	2				
				1325.1(4)	3	$5/2^-,7/2^-$	5
1344.2(8)	7	$(3/2^-,5/2^-)$[e]	(4)	1343.54(28)	100	$5/2^-$	320
				1356.6(9)	5	$(3/2^+)$[e]	4
				1365.9(6)	15	$9/2^-$	121
				1373.0(8)	6	$9/2^-$	45
				1379.2(10)	5	$1/2^+$	1
				1392.3(6)	18	$(1/2^+)$[e]	3
1394.1(6)	26	$(5/2^-,7/2^-)$[e]	8				
				1406.9(10)	2	$5/2^-$	4
				1414.8(5)	25	$5/2^+$	14
1419.0(12)	20	$(7/2^+,9/2^+)$	(17)	1419.4(6)	30	$9/2^+$	91
1430.4(6)	174	$3/2^+,5/2^+$	66	1429.5(5)	101	$5/2^+$	45
				1442.8(5)	26	$(9/2^-)$[e]	(190)
				1454.4(9)	7	$1/2^+$	2
1467.8(8)	7	$3/2^+,5/2^+$	3				
				1468.9(7)	3	$(1/2^-)$[e]	(3)
1478.1(7)	19	$3/2^+,5/2^+$	8	1478.2(5)	5	$3/2^+$	3
				1488.2(5)	17	$7/2^+$	79
1491.8(7)	31	$7/2^+,9/2^+$	33				
				1493.8(10)	3	$5/2^-,7/2^-$	5
1509.1(8)	17	$3/2^+,5/2^+$	7	1508.4(5)	37	$5/2^+$	16
1521.2(7)	103	$1/2^-,3/2^-$	28	1519.9(6)	7	$(1/2^-)$[e]	9
				1532.4(4)	12	$7/2^+$	49
1540.6(8)	39	$(3/2^+,5/2^+)$[e]	8	1541.0(5)	29	$5/2^+$	13
				1548.5(9)	2	$(3/2^+)$[e]	(3)
1560.4(7)	93	$7/2^+,9/2^+$	102				

TABLE III. (*Continued.*)

(d,p)				$(\mathbf{d},t)$			
E_x(keV)[a]	$d\sigma/d\Omega(\mu$b/sr)[b]	J^π	$S_{jl}(10^{-3})$[c]	E_x(keV)[d]	$d\sigma/d\Omega(\mu$b/sr)[b]	J^π	$G_{jl}(10^{-3})$
				1561.3(5)	16	$3/2^-$	25
1571.2(7)	48	$7/2^+,9/2^+$	44				
				1571.4(4)	100	$1/2^+$	23
1579.6(6)	1	$1/2^-,3/2^-$	8				
				1580.2(7)	54	$5/2^+$	28
1584.3(12)	39	$3/2^+,5/2^+$	10				
1593.7(8)	66	$3/2^+,5/2^+$	153	1592.5(9)	8	$5/2^+$	4
1603.1(6)	582	$1/2^-,3/2^-$	186	1603.1(4)	15	$3/2^-$	25
				1611.1(8)	2	$5/2^-$	8
1621.6(7)	70	$3/2^+,5/2^+$	23				
				1622.3(4)	16	$(11/2^-)$[e]	(143)
1628.5(8)	60	$3/2^+,5/2^+$	23				
				1631.4(5)	9	$(9/2^+)$[e]	(20)
1637.7(7)	105	$(1/2^-,3/2^-)$[e]	(44)	1637.9(7)	6	$(3/2^-)$[e]	8
				1644.1(8)	4	$5/2^-$	13
1646.2(8)	69	$3/2^+,5/2^+$	21				
1655.7(11)	68	$3/2^+,5/2^+$	23	1656.2(6)	35	$3/2^+$	16
1668.1(8)	51	$3/2^+,5/2^+$	18	1668.4(7)	25	$5/2^+$	9
				1672.9(7)	4	$(7/2^+)$[e]	(20)
1675.5(10)	37	$3/2^+,5/2^+$	13				
				1682.9(6)	1	$5/2^-,7/2^-$	5
1685.4(8)	31	$3/2^+,5/2^+$	12				
				1690.8(6)	22	$5/2^+$	9
1693.5(6)	96	$(5/2^-,7/2^-)$[e]	(31)				
1702.1(6)	52	$5/2^-,7/2^-$	16	1702.8(5)	12	$7/2^-$	21
1713.7(11)				1713.0(15)	2	$(5/2^+)$[e]	(1)
1718.7(8)	35	$3/2^+,5/2^+$	10	1719.5(12)	2	$(3/2^+)$[e]	(2)
1728.3(12)	14	$5/2^-,7/2^-$	3	1729.7(7)	3	$5/2^-$	10
1745.1(10)	10	$(3/2^+,5/2^+)$[e]	(5)	1745.9(9)	2	$(5/2^+)$[e]	(1)
1751.0(10)		$7/2^+,9/2^+$	44				
				1753.6(12)	3	$1/2^+$	1
1759.0(9)	12	$1/2^-,3/2^-$	4	1759.8(8)	1	$3/2^-$	1
				1773.8(7)	5	$3/2^-$	8
1783.2(9)	104	$1/2^-,3/2^-$	34				
				1783.8(7)	6	$(7/2^-)$[e]	15
				1792.0(9)	2	$(1/2^+)$[e]	1
				1807.2(10)	4	$7/2^-$	9
1809.2(12)	54	$5/2^-,7/2^-$	16				
1813.4(12)	54	$(3/2^+,5/2^+)$[e]	13	1813.4(7)	25	$3/2^+$	12
				1823.8(18)	2	$1/2^-$	3
1826.2(9)	20	$1/2^+$	7				
				1830.8(4)	5	$3/2^+$	2
				1840.0(8)	90	$1/2^+$	19
1846.6(8)	28	$5/2^-,7/2^-$	8				
				1850.8(19)	4	$1/2^+$	1
				1859.4(17)	3	$5/2^-$	7
1874.2(10)	14	$(3/2^+,5/2^+)$[e]	(6)	1868.2(8)	17	$3/2^+,5/2^+$	8

TABLE III. (*Continued.*)

(d,p)				$(\mathbf{d},t)$			
E_x(keV)[a]	$d\sigma/d\Omega(\mu$b/sr)[b]	J^π	$S_{jl}(10^{-3})$[c]	E_x(keV)[d]	$d\sigma/d\Omega(\mu$b/sr)[b]	J^π	$G_{jl}(10^{-3})$
				1874.2(10)	12	$5/2^+$	5
1885.4(7)	21	$1/2^-,3/2^-$	6	1883.5(8)	18	$(1/2^-)$[e]	(20)
				1891.4(23)	5	$3/2^+,5/2^+$	2
1892.0(8)	54	$1/2^-,3/2^-$	20				
				1899.8(10)	8	$3/2^+,5/2^+$	3
				1908.5(9)	10	$5/2^+$	2
1910.4(17)	10	$(1/2^-,3/2^-)$[e]	4				
				1917.5(7)	12	$3/2^+$	4
1918.4(8)	26	$(1/2^-,3/2^-)$[e]	10				
				1925.9(15)	5	$(1/2^-,3/2^-)$[e]	(2)
1927.9(8)	25	$1/2^-,3/2^-$	8				
				1930.6(14)	3	$5/2^-$	11
1933.3(11)	25	$5/2^-,7/2^-$	6				
				1938.4(7)	7	$(7/2^+)$[e]	25
				1946.1(8)	6	$1/2^-$	5
				1954.6(5)	7	$3/2^-$	9
1958.1(6)	50	$1/2^-,3/2^-$	14				
				1964.6(3)	405	$5/2^+$	146
1971.0(9)	26	$(1/2^+)$[e]	(14)				
				1972.5(8)	30	$5/2^+$	11
				1980.3(10)	26	$1/2^+$	5
1983.0(8)	152	$1/2^+$	80				
				1989.2(19)	6	$3/2^-$	8
				1997.3(7)	71	$1/2^+$	15
1997.3(7)	197	$1/2^-,3/2^-$	56				
2003.2(8)	25	$3/2^+,5/2^+$	7				
				2006.5(14)	12	$5/2^-$	26
2011.1(9)	48	$(1/2^-,3/2^-)$[e]	(20)	2012.9(14)	5	$3/2^-$	8
2032.6(10)	22	$(5/2^-,7/2^-)$[e]	(5)	2032.7(5)	73	$5/2^+$	28
				2039.3(5)	59	$3/2^+$	25
2042.0(6)	77	$(3/2^+,5/2^+)$[e]	(17)				
				2044.5(15)	17	$5/2^-$	42
2048.7(6)	173	$(1/2^-,3/2^-)$[e]	(41)				
				2051.9(9)	16	$1/2^+$	4
2058.0(8)	222	$5/2^-,7/2^-$	51				
				2073.7(6)	21	$1/2^-,3/2^-$	24
2074.1(6)	38	$(5/2^-,7/2^-)$[e]	(11)				
				2081.9(8)	14	$1/2^+$	20
2088.1(10)	27	$(3/2^+,5/2^+)$	(12)				
2092.0(12)	29	$(3/2^+,5/2^+)$[e]	(5)	2092.7(8)	76	$5/2^+$	27
2100.8(8)	25	$1/2^-,3/2^-$	8				
				2105.1(6)	31	$3/2^+$	13
				2115.1(10)	21	$3/2^-$	18
2121.7(12)	63	$5/2^-,7/2^-$	14				
				2125.8(14)	6	$3/2^-$	9
				2136.0(7)	15	$3/2^+,5/2^+$	7
				2149.9(9)	25	$5/2^+$	10

TABLE III. (*Continued.*)

(d,p)				$(\mathbf{d},t)$			
E_x(keV)[a]	$d\sigma/d\Omega(\mu$b/sr)[b]	J^π	$S_{jl}(10^{-3})$[c]	E_x(keV)[d]	$d\sigma/d\Omega(\mu$b/sr)[b]	J^π	$G_{jl}(10^{-3})$
				2162.0(20)	24	$5/2^+$	10
				2169.0(20)	16	$3/2^+$	7
				2176.0(20)	8	$(5/2^+)$[e]	6
				2186.0(20)	11	$5/2^+$	7
				2194.3(11)	22	$3/2^+$	10
				2203.1(11)	22	$3/2^+$	10
				2212.8(9)	23	$5/2^+$	10
				2221.7(10)	8	$5/2^-$	7
				2233.1(12)	5	$3/2^-$	8
				2242.3(7)	93	$5/2^+$	30
				2252.8(16)	32	$5/2^+$	12
				2260.2(8)	12	$3/2^+$	7
				2271.9(21)	8	$5/2^+$	3
				2284.5(15)	11	$3/2^+$	6
				2297.3(12)	15	$3/2^+$	7
				2306.0(20)	7	$3/2^+$	6
				2316.6 (12)	21	$3/2^-, 5/2^-$	11

[a]Values averaged over all spectra. A systematic error of 0.5 keV is included.
[b]Values given at $\theta_{\text{lab}}=30°$.
[c]For levels with ambiguous j assignment, the values shown correspond to the smaller j value (i.e., $j=l-1$). The S_{jl} values for the larger j values are derived from the ratios $1/2^-:3/2^-=2.0$, $3/2^+:5/2^+=1.65$, $5/2^-:7/2^-=1.55$, $7/2^+:9/2^+=1.85$, $9/2^-:11/2^-=1.9$, and $11/2^+:13/2^+=2.5$ (about 5% error).
[d]Values averaged over all spectra. A systematic error of 0.2 keV is included.
[e]Irregular DWBA fit.
[f]Based on the measurement at 40°.
[g]Assuming same spin and parity of $(\mathbf{d},t)$.
[h]Based on the measurement at 20° with unpolarized deuteron beam.
[i]Assuming l values taken from (d,p) and j values taken from final assignments (see Table IV).
[j]Assuming J^π from construction of rotational band.

Level assignments above 1.2 MeV should be considered as tentative. The level density increases with increasing level energy and the experimental information on spin and parity between different experiments becomes less compatible. In addition, the model structure of the levels becomes more complex with increasing excitation energy and, therefore, the interpretation of experimental data becomes more uncertain. In the following, states are characterized by the main Nilsson component and also by the dominant vibrational admixture (if there is any) in terms of the quasiparticle-phonon model.

All levels observed below 700 keV have been arranged into rotational bands. New levels below 1 MeV are observed at 324.9, 330.479, 633.60, 684.16, 835.5, 876.5, 880.63, 915.828, and 938.7 keV. The 710.38 and 732.87 keV levels, reported in γ-γ coincidences in β^- decay of ^{159}Eu [10], are confirmed by secondary γ rays in radiative neutron capture (see Table V). The level 710.38 keV is assigned to the band $\frac{3}{2}[651]$ (see Sec. IV C). Levels with new assignments include the previously unresolved doublet at 328 and the 855 keV level [9]. In the nucleon transfer reactions and in the (n,γ) experiments [11,12] a large number of levels are newly observed namely above 1 MeV (see Tables IV and V).

B. Rotational bands with negative parity

The $\frac{3}{2}[\mathbf{521}]$ *ground-state band.* Levels at $0.0(\frac{3}{2})$, $50.627(\frac{5}{2})$, $121.899(\frac{7}{2})$, $212.6(\frac{9}{2})$, and 324.9 keV$(\frac{11}{2})$.

This orbital also appears as the ground state in a number of neighboring nuclei, namely in ^{155,157}Sm, ^{153,155,157}Gd, ^{155,157,159}Dy, ^{157,159,161}Er, and ^{161,163}Yb [50]. We include a newly observed level at 324.9 keV as the $\frac{11}{2}$ member of this band. The angular dependence of the corresponding differential cross section could not be fitted acceptably by DWBA with any definite transferred angular momentum. The value of $l=3$ gives the best fit (see Fig. 7). The $\frac{5}{2}^-$ level at 50.627 keV is not populated by primary γ rays in any of the (n,γ) experiments [11,12] even though higher-lying $\frac{5}{2}^-$ levels, such as those at 146.316, 588.517, and 872.64 keV, are populated by primary γ rays in 24 keV neutron capture [12] (see Table IV). The weak population of this level in the transfer reactions agrees well with our model calculations.

The $\frac{5}{2}[\mathbf{523}]$ *band.* Levels at $146.316(\frac{5}{2})$, $227.412(\frac{7}{2})$, $330.479(\frac{9}{2})$, and 456.4 keV$(\frac{11}{2})$.

The $\frac{5}{2}[\mathbf{523}]$ orbital appears as the ground state in ^{161}Gd and rather as a low-lying particle state in ^{159}Gd. The previous

TABLE IV. Level scheme of ^{159}Gd. Final levels result as combination of levels observed in the transfer reactions and levels populated by primary γ rays from our previous (n,γ) experiments [11,12]. Levels reported in previous studies of (d,p), (d,t) [1], and (n,γ) [9] reactions are included for comparison.

Final		$(d,p),(\mathbf{d},t)$		(n,γ_{pri})		Previous studies	
E_x(keV)	J^π	E_x(keV)	J^π	E_x(keV)	J^π	E_x(keV)	J^π
0.0	$3/2^{-a}$	0.0	$1/2^-,3/2^-$	0.0	$1/2^-,3/2^-$	0.0	$3/2^-$
50.627(9)[b]	$5/2^{-a}$	51.1(6)	$(5/2^-,7/2^-)^c$			50.66(9)	$5/2^-$
67.829(24)[b]	$5/2^{+a}$	66.7(6)	$3/2^+,5/2^+$	67.65(6)	$5/2^+$	67.79(7)	$5/2^+$
118.686(28)[b]	$7/2^{+a}$	119.2(9)				118.92(15)	$7/2^+$
121.899(24)[b]	$7/2^{-a}$	122.1(4)	$5/2^-,7/2^-$			121.93(13)	$7/2^-$
146.316(6)[b]	$5/2^{-a}$	146.1(4)	$5/2^-,7/2^-$	146.94(23)	$5/2^-$	146.39(8)	$5/2^-$
185.0(4)	$9/2^{+a}$	185.0(4)	$7/2^+,9/2^+$			185.4(4)	$9/2^+$
212.6(6)	$9/2^{-a}$	212.6(4)	$9/2^-,11/2^-$			212.30(23)	$9/2^-$
227.412(21)[b]	$7/2^{-a}$	227.6(4)	$5/2^-,7/2^-$			227.49(10)	$7/2^-$
273.9(6)	$11/2^{+a}$	273.9(6)	$11/2^+,13/2^+$			273.0(2)	$(11/2^+)$
324.9(5)	$11/2^{-a}$	324.9(5)	$9/2^-,11/2^-$				
330.479(13)[b]	$9/2^{-a}$	330.8(5)	$9/2^-,11/2^-$			328.0(3)	$9/2^-,11/2^-$
372.7(4)	$13/2^{+a}$	372.7(4)	$11/2^+,13/2^+$			372.0(2)	$13/2^+$
456.4(5)	$11/2^{-a}$	456.4(5)	$9/2^-,11/2^-$			456.0(2)	$11/2^-$
507.724(16)[b]	$1/2^{-a}$	508.1(4)	$1/2^-,3/2^-$	507.75(5)	$1/2^-,3/2^-$	507.7(3)	$1/2^-$
558.211(12)[b]	$3/2^{-a}$	558.0(6)	$(1/2^-,3/2^-)^c$	558.36(3)	$1/2^-,3/2^-$	558.2(2)	$3/2^-$
588.517(27)[b]	$5/2^{-a}$	588.8(5)	$5/2^-,7/2^-$	589.7(6)	$5/2^-$	589.0(3)	$5/2^-$
601.977(9)[b]	$3/2^{+a}$	602.0(9)	$3/2^+,5/2^+$	601.87(7)	$1/2^+,3/2^+$	602.13(17)	$(3/2^+)$
633.60(12)[b]	$7/2^{+a}$	633.2(6)	$7/2^+,9/2^+$				
646.697(23)[b]	$5/2^{+a}$	646.5(10)	$3/2^+,5/2^+$	646.93(10)	$5/2^+$	647.2(2)	$(5/2^+)$
684.16(25)	$11/2^{-a}$	684.16(25)	$11/2^{-c}$			681.0(10)	$11/2^-$
705.3(4)	$7/2^{-a}$	705.3(4)	$7/2^-$			705.0(2)	$7/2^-$
710.38(8)[b,d]	$7/2^{+a}$						
732.87(5)[b,d]	$(5/2^-,7/2^-)$						
744.378(16)[b]	$3/2^{+a}$	744.22(27)	$3/2^+$	744.48(7)	$1/2^+,3/2^+$	744.38(11)	$3/2^+$
759.8(8)	$9/2^{-a}$	759.8(8)	$(9/2^-,11/2^-)^c$			761.0(5)	$9/2^-$
781.556(17)[b]	$1/2^{+a}$	781.35(23)	$1/2^+$	782.08(8)	$1/2^+,3/2^+$	782.3(6)	$1/2^+$
800.45(4)[b]	$5/2^{+a}$	800.4(6)	$3/2^+,5/2^+$	800.59(11)	$5/2^+$	801.0(15)	$(5/2)^+$
818.89(7)[b]	$5/2^{+a}$	819.4(7)	$3/2^+,5/2^+$	818.59(15)	$5/2^+$	818.2(14)	$(5/2)^+$
819.5(8)	$11/2^+,13/2^+$	819.5(8)	$11/2^+,13/2^+$				
835.5(8)	$9/2^{+a}$	835.5(8)	$(7/2^+,9/2^+)$			837.0(5)	
858.51(7)[b]	$3/2^{+a}$	858.7(5)	$3/2^+$	858.53(10)	$1/2^+,3/2^+$	859.7(20)	$(5/2)^+$
872.64(5)[b]	$5/2^{-a}$			872.71(25)	$5/2^-$	872.70(14)	$5/2^-$
874.5(11)	$(1/2^+)$	874.5(11)	$(1/2^+)^c$				
876.5(4)	$7/2^{+a}$	876.5(4)	$(7/2^+,9/2^+)^c$				
880.63(24)[b]	$1/2^+,3/2^+,5/2^+$			880.4(4)	$1/2^+,3/2^+,5/2^+$		
915.828(10)[b]	1/2,3/2			915.3(6)	1/2,3/2		
926.63(29)	$7/2^-$	926.63(29)	$7/2^-$			924	
938.7(5)	$11/2^{-a}$	938.7(5)	$(9/2^-,11/2^-)^c$				
948.35(28)[b]	$7/2^{-a}$	948.8(4)	$7/2^-$			948.50(22)	$7/2^-$
962.4(6)	$3/2^+$	962.4(6)	$3/2^+$				
974.29(5)[b]	$1/2^{+a}$	974.2(5)	$1/2^+$	974.39(8)	$1/2^+,3/2^+$	973.7(4)	$1/2^+$
1001.62(13)[b]	$3/2^{+a}$	1001.53(23)	$3/2^+$	1001.55(12)	$1/2^+,3/2^+$	1001.6(5)	$3/2^+$
1014.9(8)	$1/2^+$	1014.9(8)	$1/2^+$				
1043.2(5)	$9/2^{-a}$	1043.2(5)	$9/2^-,11/2^-$			1044.0(5)	$(9/2^-)$
1059.6(5)	$5/2^{+a}$	1059.6(5)	$5/2^+$				

TABLE IV. (*Continued.*)

Final		$(d,p),(\mathbf{d},t)$		(n,γ_{pri})		Previous studies	
E_x(keV)	J^π	E_x(keV)	J^π	E_x(keV)	J^π	E_x(keV)	J^π
1061.70(7)[b]	$1/2^-,3/2^-$			1061.85(7)	$1/2^-,3/2^-$	1060.9(8)	$1/2,3/2$
1079.39(4)[b]	$1/2^-$	1079.9(4)	$1/2^-$	1079.50(4)	$1/2^-,3/2^-$	1079.3(1)	$(1/2,3/2)^-$
1093.0(7)	$13/2^{+a}$	1093.0(7)	$11/2^+,13/2^+$				
1110.25(7)[b]	$3/2^{-a}$	1110.66(25)	$3/2^-$	1110.39(8)	$1/2^-,3/2^-$	1110.7(1)	$3/2^-$
1120.3(5)	$7/2^{+a}$	1120.3(5)	$7/2^+$				
1128.73(6)[b]	$1/2^{+d}$			1128.59(11)	$1/2^+,3/2^+$	1128.52(21)	$(1/2,3/2)^+$
1128.8(5)	$3/2^+$	1128.8(5)	$3/2^+$				
1134.7(4)	$7/2^{-a}$	1134.7(4)	$7/2^-$				
1139.84(4)[b]	$1/2^{-a}$	1139.81(27)	$1/2^-$	1140.08(10)	$1/2^-,3/2^-$	1139.0(5)	$(1/2^+,3/2^+)$
1145.60(6)[b]	$3/2^{-a}$	1146.02(25)	$3/2^-$	1145.99(8)	$1/2^-,3/2^-$	1145.4(4)	$3/2^-$
1151.0(9)	$(1/2^+)$	1151.0(9)	$(1/2^+)$[c]				
1159.90(8)[b]	$5/2^+$	1159.98(25)	$5/2^+$	1159.59(21)	$5/2^+$	1160.0(5)	$(1/2,3/2,5/2)^+$
1170.9(4)	$1/2^+$			1170.9(4)	$1/2^+$		
1178.4(6)	$1/2^+,3/2^+,5/2^+$			1178.4(6)	$1/2^+,3/2^+,5/2^+$	1179.6(10)	$(5/2)^+$
1178.6(5)	$5/2^{-a}$	1178.6(5)	$5/2^-$				
1190.5(6)	$5/2^+$	1190.5(6)	$5/2^+$				
1194.2(8)	$7/2^+,9/2^+$	1194.2(8)	$7/2^+,9/2^+$				
1202.6(5)	$9/2^+$	1202.6(5)	$9/2^+$			1202.0(3)	$(5/2^-,7/2^-)$
1203.5(7)	$9/2^{-a}$	1203.5(7)	$9/2^-,11/2^-$				
1216.9(8)	$1/2^-$	1216.9(8)	$1/2^-$				
1229.3(5)	$9/2^{+a}$	1229.3(5)	$9/2^+$				
1239.4(4)	$7/2^{-a}$	1239.4(4)	$7/2^{-c}$			1238.0(3)	$(7/2^-)$
1253.1(5)	$5/2^{-a}$	1253.1(5)	$5/2^-$			1250	
1283.8(6)	$(7/2^+,9/2^+)$	1283.8(6)	$(7/2^+,9/2^+)$[c]			1282	$(7/2^+)$
1284.38(12)	$3/2^-$	1284.1(4)	$3/2^-$	1284.45(13)	$1/2,3/2$	1283.9	$(1/2,3/2)^+$
1296.5(5)	$3/2^-$	1296.5(5)	$1/2^+$				
1303.4(4)	$7/2^{-a}$	1303.4(4)	$7/2^-$			1301.0(5)	$(9/2^-)$
1315.80(28)	$1/2^+$	1315.80(28)	$1/2^+$				
1322.2(11)	$(3/2^+,5/2^+)$	1322.2(11)	$(3/2^+,5/2^+)$				
1325.12(27)	$5/2^-$	1325.10(28)	$5/2^-,7/2^-$	1325.3(8)	$1/2,3/2,5/2$		
1343.82(21)	$5/2^-$	1343.71(26)	$5/2^-$	1344.0(4)	$1/2^+,3/2^+,5/2^+$	1341	$(9/2^-)$
1356.6(9)	$(3/2^+)$	1356.6(9)	$(3/2^+)$[c]				
1365.9(6)	$9/2^{-a}$	1365.9(6)	$9/2^-$			1365	
1373.0(8)	$9/2^-$	1373.0(8)	$9/2^-$				
1379.2(10)	$1/2^+$	1379.2(10)	$1/2^+$				
1392.3(6)	$(1/2^+)$	1392.3(6)	$(1/2^+)$[c]			1392.6(10)	$(1/2,3/2)^+$
1394.1(6)	$(5/2^-,7/2^-)$	1394.1(6)	$(5/2^-,7/2^-)$[c]				
1394.45(15)	$1/2^+,3/2^+$			1394.45(15)	$1/2^+,3/2^+$		
1400.2(5)	$1/2^-,3/2^-$			1400.2(5)	$1/2^-,3/2^-$	1400.0(12)	$(1/2,3/2)^+$
1406.9(10)	$5/2^-$	1406.9(10)	$5/2^-$				
1414.8(5)	$5/2^+$	1414.8(5)	$5/2^+$			1415	
1418.4(4)	$1/2^+,3/2^+$			1418.4(4)	$1/2^+,3/2^+$		
1419.3(5)	$9/2^+$	1419.3(5)	$9/2^+$				
1430.95(16)	$3/2^+,5/2^+$	1429.9(4)	$5/2^+$	1431.24(17)	$1/2^+,3/2^+$	1424.0(4)	$3/2^+,5/2^+$
1442.8(5)	$9/2^{-a}$	1442.8(5)	$(9/2^-)$[c]				
1446.5(6)	$1/2^+,3/2^+$			1446.5(6)	$1/2^+,3/2^+$	1446.7(14)	$(1/2,3/2)^+$
1554.4(9)	$1/2^+$	1454.4(9)	$1/2^+$				

TABLE IV. (*Continued.*)

Final		$(d,p),(\mathbf{d},t)$		$(n,\gamma_{\mathrm{pri}})$		Previous studies	
E_x(keV)	J^π	E_x(keV)	J^π	E_x(keV)	J^π	E_x(keV)	J^π
1468.31(17)	$3/2^+$	1467.8(8)	$3/2^+,5/2^+$	1468.33(18)	$1/2^+,3/2^+$	1467.1(12)	$(1/2,3/2)^+$
1468.9(7)	$(1/2^-)$	1468.9(7)	$(1/2^-)^c$				
1477.79(11)	$3/2^+$	1478.2(4)	$3/2^+$	1477.75(11)	$1/2^+,3/2^+$	1477.8(9)	$(1/2^+,3/2^+)$
1488.2(5)	$7/2^{+a}$	1488.2(5)	$7/2^+$				
1491.8(7)	$7/2^+,9/2^+$	1491.8(7)	$7/2^+,9/2^+$				
1493.8(10)	$5/2^-,7/2^-$	1493.8(10)	$5/2^-,7/2^-$			1493	
1505.1(7)	$1/2^{(+)},3/2^{(+)}$			1505.1(7)	$1/2^{(+)},3/2^{(+)}$		
1508.6(4)	$5/2^+$	1508.6(4)	$5/2^+$				
1520.86(11)	$1/2^-$	1520.4(5)	$1/2^-$	1520.90(12)	$1/2^-,3/2^-$	1519.81(117)	$(3/2^-)$
1532.4(4)	$7/2^+$	1532.4(4)	$7/2^+$				
1540.46(26)	$5/2^+$	1540.9(4)	$5/2^+$	1540.1(4)	$1/2^+,3/2^+,5/2^+$	1538.4	$(1/2,3/2,5/2)^+$
1545.5(3)	$1/2,3/2$			1545.5(3)	$1/2,3/2$	1545.3(1)	$(1/2,3/2,5/2)^+$
1548.5(9)	$(3/2^+)$	1548.5(9)	$(3/2^+)^c$				
1557.1(10)	$1/2^+,3/2^+$			1557.1(10)	$1/2^+,3/2^+$		
1560.4(7)	$7/2^+,9/2^+$	1560.4(7)	$7/2^+,9/2^+$				
1560.62(10)	$3/2^-$	1561.3(5)	$3/2^-$	1560.58(10)	$1/2^-,3/2^-$	1560.9(8)	$(1/2^+,3/2^+)$
1571.2(7)	$7/2^+,9/2^+$	1571.2(7)	$7/2^+,9/2^+$				
1571.91(12)	$1/2^+$	1571.4(4)	$1/2^+$	1571.97(12)	$1/2,3/2$	1572.1(10)	$(1/2^+,3/2^+)$
1579.21(19)	$1/2^+,3/2^+$			1579.21(19)	$1/2^+,3/2^+$	1581.9(12)	$(1/2,3/2)^+$
1579.6(6)	$1/2^{-a}$	1579.6(6)	$1/2^-,3/2^-$				
1580.2(7)	$5/2^+$	1580.2(7)	$5/2^+$				
1582.3(9)	$1/2^{(-)},3/2^{(-)}$			1582.3(9)	$1/2^{(-)},3/2^{(-)}$		
1584.51(17)	$3/2^+$	1584.3(12)	$3/2^+,5/2^+$	1584.51(17)	$1/2^+,3/2^+$		
1593.12(19)	$1/2^+,3/2^+$			1593.12(19)	$1/2^+,3/2^+$		
1593.2(6)	$5/2^+$	1593.2(6)	$5/2^+$				
1603.30(10)	$3/2^{-a}$	1603.09(28)	$3/2^-$	1603.34(11)	$1/2^-,3/2^-$	1603.2(2)	$(3/2^-)$
1611.1(8)	$5/2^-$	1611.1(8)	$5/2^-$				
1615.1(6)	$1/2^+,3/2^+$			1615.1(6)	$1/2^+,3/2^+$		
1621.6(7)	$3/2^+,5/2^+$	1621.6(7)	$3/2^+,5/2^+$				
1622.3(4)	$11/2^{-a}$	1622.3(4)	$(11/2^-)^c$				
1627.2(4)	$5/2^+$	1628.5(8)	$3/2^+,5/2^+$	1626.7(5)	$5/2$	1625.5(8)	$(1/2,3/2,5/2)^+$
1631.4(5)	$(9/2^+)$	1631.4(5)	$(9/2^+)^c$				
1635.0(10)	$1/2^+,3/2^+$			1635.0(10)	$1/2^+,3/2^+$		
1637.8(5)	$3/2^{-a}$	1637.8(5)	$(3/2^-)^c$			1638	$(5/2^-)$
1642.50(10)	$1/2^-,3/2^-$			1642.50(10)	$1/2^-,3/2^-$	1642.0(6)	$(1/2,3/2)^-$
1644.1(8)	$5/2^-$	1644.1(8)	$5/2^-$				
1646.2(8)	$3/2^+,5/2^+$	1646.2(8)	$3/2^+,5/2^+$				
1656.6(4)	$3/2^+$	1656.1(5)	$3/2^+$	1657.0(5)	$1/2^+,3/2^+$	1655.0(12)	$(1/2,3/2)^+$
1668.3(5)	$5/2^+$	1668.3(5)	$5/2^+$				
1669.8(15)	$1/2^{(+)},3/2^{(+)}$			1669.8(15)	$1/2^{(+)},3/2^{(+)}$		
1672.9(7)	$(7/2^+)$	1672.9(7)	$(7/2^+)^c$			1670	
1673.31(11)	$1/2^-,3/2^-$			1673.31(11)	$1/2^-,3/2^-$	1673.5(6)	$(1/2,3/2)^-$
1675.5(10)	$3/2^+,5/2^+$	1675.5(10)	$3/2^+,5/2^+$				
1682.9(6)	$5/2^-,7/2^-$	1682.9(6)	$5/2^-,7/2^-$				
1685.4(8)	$3/2^+,5/2^+$	1685.4(8)	$3/2^+,5/2^+$				
1690.6(5)	$5/2^+$	1690.8(6)	$5/2^+$	1690.2(7)	$5/2$		
1693.5(6)	$5/2^{-a}$	1693.5(6)	$(5/2^-,7/2^-)^c$			1692	

TABLE IV. (*Continued.*)

Final		$(d,p),(\mathbf{d},t)$		(n,γ_{pri})		Previous studies	
E_x(keV)	J^π	E_x(keV)	J^π	E_x(keV)	J^π	E_x(keV)	J^π
1702.5(4)	$7/2^-$	1702.5(4)	$7/2^-$				
1704.6(10)	1/2,3/2			1704.6(10)	1/2,3/2	1706.2(11)	$(1/2,3/2)^+$
1713.2(15)	$(5/2^+)$	1713.2(15)	$(5/2^+)^c$				
1719.1(12)	$(3/2^+)$	1719.1(12)	$(3/2^+)^c$				
1721.74(19)	1/2,3/2			1721.74(19)	1/2,3/2	1722.4(12)	$(1/2,3/2)^+$
1729.4(6)	$5/2^-$	1729.4(6)	$5/2^-$			1730.0(1)	$(5/2)^+$
1745.7(5)	$(5/2^+)$	1745.7(5)	$(5/2^+)^c$				
1746.0(8)	$1/2^+,3/2^+$			1746.0(8)	$1/2^+,3/2^+$	1747.0(12)	$(1/2,3/2)^+$
1751.0(10)	$7/2^+,9/2^+$	1751.0(10)	$7/2^+,9/2^+$			1751.0(5)	$(7/2^-)$
1753.6(12)	$1/2^+$	1753.6(12)	$1/2^+$				
1758.69(10)	$3/2^-$	1759.5(6)	$3/2^-$	1758.66(10)	$1/2^-,3/2^-$	1757.9	$(1/2,3/2)^-$
1772.57(14)	1/2,3/2			1772.57(14)	1/2,3/2		
1773.8(7)	$3/2^-$	1773.8(7)	$3/2^-$				
1774.1(6)	5/2			1774.1(6)	5/2	1773.7	1/2,3/2,5/2
1782.53(11)	$1/2^-,3/2^-$	1783.2(9)	$1/2^-,3/2^-$	1782.52(11)	$1/2^-,3/2^-$	1781.9	$(1/2,3/2)^-$
1783.8(7)	$(7/2^-)$	1783.8(7)	$(7/2^-)^c$				
1792.0(9)	$(1/2^+)$	1792.0(9)	$(1/2^+)^c$				
1807.2(10)	$7/2^-$	1807.2(10)	$7/2^-$				
1808.50(29)	1/2,3/2			1808.50(29)	1/2,3/2		
1809.2(12)	$5/2^-,7/2^-$	1809.2(12)	$5/2^-,7/2^-$			1809	
1813.4(6)	$3/2^+$	1813.4(6)	$3/2^+$				
1825.27(16)	$1/2^-$	1823.8(18)	$1/2^-$	1825.28(16)	$1/2^-,3/2^-$		
1826.2(9)	$1/2^+$	1826.2(9)	$1/2^+$				
1830.99(19)	$3/2^+$	1830.8(7)	$3/2^+$	1831.5(4)	1/2,3/2		
1840.0(7)	$1/2^+$	1840.0(8)	$1/2^+$			1839	$(3/2^+)$
1840.9(15)	$1/2^-,3/2^-$			1840.9(15)	$1/2^-,3/2^-$	1839	$(3/2^+)$
1841.0(3)	5/2			1841.0(3)	5/2	1839	$(3/2^+)$
1846.6(8)	$5/2^-,7/2^-$	1846.6(8)	$5/2^-,7/2^-$				
1851.9(5)	$1/2^+$	1850.8(16)	$1/2^+$	1852.3(5)	$1/2^+,3/2^+,5/2^+$		
1859.4(14)	$5/2^-$	1859.4(14)	$5/2^-$				
1869.02(19)	$3/2^+$	1868.4(6)	$3/2^+,5/2^+$	1869.09(20)	$1/2^+,3/2^+$	1867	
1872.7(6)	$5/2^+$	1874.2(12)	$5/2^+$	1872.4(6)	5/2		
1880.7(10)	1/2,3/2			1880.7(10)	1/2,3/2		
1883.66(9)	$1/2^-$	1884.6(7)	$1/2^-$	1883.64(9)	$1/2^-,3/2^-$	1885	
1891.26(21)	$3/2^+,5/2^+$	1891.4(9)	$3/2^+,5/2^+$	1890.5(6)	1/2,3/2,5/2		
1892.0(8)	$1/2^-,3/2^-$	1892.0(8)	$1/2^-,3/2^-$				
1896.8(30)	$1/2^{(+)},3/2^{(+)}$			1896.8(30)	$1/2^{(+)},3/2^{(+)}$	1896	(1/2,3/2)
1900.1(4)	$3/2^+$	1899.8(10)	$3/2^+,5/2^+$	1900.1(4)	$1/2^+,3/2^+$		
1908.5(9)	$5/2^+$	1908.5(9)	$5/2^+$			1909	
1910.4(17)	$(1/2^-,3/2^-)$	1910.4(17)	$(1/2^-,3/2^-)^c$				
1917.5(7)	$3/2^+$	1917.5(7)	$3/2^+$				
1917.6(5)	5/2			1917.6(5)	5/2		
1918.4(8)	$(1/2^-,3/2^-)$	1918.4(8)	$(1/2^-,3/2^-)^c$	1918.5(10)	1/2,3/2	1922	
1925.9(15)	$(1/2^-,3/2^-)$	1925.9(15)	$(1/2^-,3/2^-)^c$				
1926.0(9)	$1/2^{(+)},3/2^{(+)}$			1926.0(9)	$1/2^{(+)},3/2^{(+)}$		
1927.9(8)	$1/2^-,3/2^-$	1927.9(8)	$1/2^-,3/2^-$				
1930.6(14)	$5/2^-$	1930.6(14)	$5/2^-$				

TABLE IV. (*Continued.*)

Final		$(d,p),(\mathbf{d},t)$		$(n,\gamma_{\mathrm{pri}})$		Previous studies	
E_x(keV)	J^π	E_x(keV)	J^π	E_x(keV)	J^π	E_x(keV)	J^π
1933.3(11)	$5/2^-,7/2^-$	1933.3(11)	$5/2^-,7/2^-$				
1938.4(7)	$(7/2^+)$	1938.4(7)	$(7/2^+)^c$				
1945.88(23)	$1/2^-$	1946.1(8)	$1/2^-$	1945.85(24)	$1/2^-,3/2^-$		
1954.50(22)	$3/2^-$	1954.6(5)	$3/2^-$	1954.46(25)	$1/2,3/2$	1953	
1958.1(6)	$1/2^-,3/2^-$	1958.1(6)	$1/2^-,3/2^-$			1960	$(7/2^+)$
1964.6(4)	$5/2^+$	1964.6(4)	$5/2^+$				
1971.47(18)	$1/2^{(+)}$	1971.0(9)	$(1/2^+)^c$	1971.49(18)	$1/2^{(-)},3/2^{(-)}$		
1972.5(8)	$5/2^+$	1972.5(8)	$5/2^+$				
1980.3(10)	$1/2^+$	1980.3(10)	$1/2^+$	1981.6(10)	$1/2^+,3/2^+$	1978	$(1/2^+)$
1983.3(8)	$1/2^{+a}$	1983.0(8)	$1/2^+$	1983.5(5)	$1/2^+,3/2^+$		
1989.2(19)	$3/2^-$	1989.2(19)	$3/2^-$			1992	$(3/2^+)$
1996.4(4)	$5/2$			1996.4(4)	$5/2$		
1997.3(7)	$1/2^+$	1997.3(7)	$1/2^+$				
1997.3(6)	$3/2^{-a}$	1997.3(6)	$1/2^-,3/2^-$				
2003.2(8)	$3/2^{+a}$	2003.2(8)	$3/2^+,5/2^+$				
2006.5(14)	$5/2^-$	2006.5(14)	$5/2^-$			2007	
2007.5(4)	$1/2^+,3/2^+$			2007.5(4)	$1/2^+,3/2^+$		
2011.66(13)	$3/2^-$	2012.2(8)	$3/2^-$	2011.65(14)	$1/2^-,3/2^-$		
2032.7(4)	$5/2^{(+)}$	2032.7(4)	$5/2^{(+)}$			2030	
2033.00(18)	$1/2^-,3/2^-$			2033.00(18)	$1/2^-,3/2^-$		
2038.3(17)	$1/2^-,3/2^-$			2038.3(17)	$1/2^-,3/2^-$		
2039.63(15)	$3/2^+$	2039.3(5)	$3/2^+$	2039.68(16)	$1/2^+,3/2^+$		
2042.0(6)	$(3/2^+,5/2^+)$	2042.0(6)	$(3/2^+,5/2^+)^c$			2042	$(5/2^+)$
2044.5(15)	$5/2^-$	2044.5(15)	$5/2^-$				
2048.7(6)	$1/2^{-a}$	2048.7(6)	$(1/2^-,3/2^-)^c$				
2050.91(19)	$1/2^+$	2051.9(9)	$1/2^+$	2050.86(20)	$1/2^+,3/2^+$		
2053.0(13)	$1/2^-,3/2^-$			2053.0(13)	$1/2^-,3/2^-$	2053	
2058.0(8)	$7/2^{-a}$	2058.0(8)	$5/2^-,7/2^-$				
2074.16(12)	$1/2^-,3/2^-$	2073.7(6)	$1/2^-,3/2^-$	2074.18(12)	$1/2^-,3/2^-$	2071	
2074.1(6)	$(5/2^-,7/2^-)$	2074.1(6)	$(5/2^-,7/2^-)^c$				
2081.9(8)	$1/2^+$	2081.9(8)	$1/2^+$			2081	$(7/2^+)$
2087.6(9)	$1/2^{(-)},3/2^{(-)}$			2087.6(9)	$1/2^{(-)},3/2^{(-)}$		
2088.1(10)	$5/2^{+a}$	2088.1(10)	$(3/2^+,5/2^+)$			2089	
2092.5(7)	$5/2^+$	2092.5(7)	$5/2^+$				
2100.8(6)	$1/2^-,3/2^-$	2100.8(8)	$1/2^-,3/2^-$				
2103.0(8)	$5/2$			2103.0(8)	$5/2$		
2105.1(6)	$3/2^+$	2105.1(6)	$3/2^+$			2106	
2110.6(5)	$1/2^{(-)},3/2^{(-)}$			2110.6(5)	$1/2^{(-)},3/2^{(-)}$		
2115.1(10)	$3/2^-$	2115.1(10)	$3/2^-$				
2116.7(5)	$1/2^+,3/2^+$			2116.7(5)	$1/2^+,3/2^+$		
2121.7(12)	$5/2^-,7/2^-$	2121.7(12)	$5/2^-,7/2^-$				
2121.7(5)	$1/2^{(-)},3/2^{(-)}$			2121.7(5)	$1/2^{(-)},3/2^{(-)}$		
2125.8(14)	$3/2^-$	2125.8(14)	$3/2^-$				
2134.3(12)	$1/2^{(-)},3/2^{(-)}$			2134.3(12)	$1/2^{(-)},3/2^{(-)}$	2134	
2136.8(10)	$3/2^+,5/2^+$	2136.0(7)	$3/2^+,5/2^+$	2137.6(5)	$1/2^{(+)},3/2^{(+)}$		
2149.9(10)	$5/2^+$	2149.9(10)	$5/2^+$				
2150.9(4)	$1/2,3/2$			2150.9(4)	$1/2,3/2$		

TABLE IV. (*Continued.*)

Final		$(d,p),(\mathbf{d},t)$		(n,γ_{pri})		Previous studies	
E_x(keV)	J^π	E_x(keV)	J^π	E_x(keV)	J^π	E_x(keV)	J^π
2153.4(10)	$1/2,3/2$			2153.4(10)	$1/2,3/2$		
2158.59(16)	$1/2,3/2$			2158.59(16)	$1/2,3/2$	2157	$(1/2,3/2)$
2162.0(20)	$5/2^+$	2162.0(20)	$5/2^+$				
2162.6(8)	$1/2^-,3/2^-$			2162.6(8)	$1/2^-,3/2^-$		
2165.39(17)	$1/2,3/2$			2165.39(17)	$1/2,3/2$	2166	
2169.2(20)	$3/2^+$	2169.2(20)	$3/2^+$				
2176.2(20)	$(5/2^+)$	2176.2(20)	$(5/2^+)$[c]				
2178.7(10)	$1/2^-,3/2^-$			2178.7(10)	$1/2^-,3/2^-$		
2182.39(12)	$1/2^-,3/2^-$			2182.39(12)	$1/2^-,3/2^-$		
2186.0(20)	$5/2^+$	2186.0(20)	$5/2^+$				
2187.98(23)	$1/2^-,3/2^-$			2187.98(23)	$1/2^-,3/2^-$		
2190.8(14)	$1/2^{(-)},3/2^{(-)}$			2190.8(14)	$1/2^{(-)},3/2^{(-)}$		
2193.8(5)	$3/2^+$	2194.3(11)	$3/2^+$	2193.7(6)	$1/2^+,3/2^+$	2194	$(1/2,3/2)$
2200.8(10)	$1/2^{(-)},3/2^{(-)}$			2200.8(10)	$1/2^{(-)},3/2^{(-)}$		
2203.1(11)	$3/2^+$	2203.1(11)	$3/2^+$				
2203.8(4)	$5/2$			2203.8(4)	$5/2$		
2206.6(10)	$1/2,3/2$			2206.6(10)	$1/2,3/2$		
2210.67(27)	$1/2^-,3/2^-$			2210.67(27)	$1/2^-,3/2^-$		
2212.8(9)	$5/2^+$	2212.8(9)	$5/2^+$				
2215.01(27)	$1/2,3/2$			2215.01(27)	$1/2,3/2$		
2222.0(4)	$5/2^-$	2221.7(10)	$5/2^-$	2222.0(5)	$1/2,3/2,5/2$		
2234.32(14)	$3/2^-$	2233.1(12)	$3/2^-$	2234.34(14)	$1/2^-,3/2^-$		
2242.3(7)	$5/2^+$	2242.3(7)	$5/2^+$			2238	
2252.4(27)	$1/2^+,3/2^+$			2252.41(27)	$1/2^+,3/2^+$		
2252.8(16)	$5/2^+$	2252.8(16)	$5/2^+$				
2257.02(14)	$1/2^-,3/2^-$			2257.02(14)	$1/2^-,3/2^-$		
2261.23(22)	$3/2^+$	2260.2(8)	$3/2^+$	2261.34(23)	$1/2^+,3/2^+$		
2271.9(21)	$5/2^+$	2271.9(21)	$5/2^+$			2274	
2280.9(7)	$1/2^-,3/2^-$			2280.9(7)	$1/2^-,3/2^-$		
2283.71(20)	$3/2^+$	2284.5(15)	$3/2^+$	2283.70(20)	$1/2^+,3/2^+$		
2287.80(18)	$1/2^-,3/2^-$			2287.80(18)	$1/2^-,3/2^-$		
2297.3(12)	$3/2^+$	2297.3(12)	$3/2^+$			2295	$(1/2,3/2)$
2300.8(4)	$1/2^+,3/2^+$			2300.8(4)	$1/2,3/2$		
2303.6(4)	$5/2$			2303.6(4)	$5/2$		
2306.0(20)	$3/2^+$	2306.0(20)	$3/2^+$				
2315.22(17)	$1/2^-,3/2^-$			2315.22(17)	$1/2^-,3/2^-$		

[a]From construction of rotational bands (see Sec. IV).
[b]Accurate values determined by χ^2 fit of secondary γ rays (see Table V).
[c]Anomalous DWBA fit of differential cross section.
[d]Determined by placement of secondary γ rays.

identification of the levels of this rotational band [1] is confirmed. The spectroscopic factors observed in the (d,p) reaction for this band are in reasonable agreement with our Coriolis band mixing calculations. The levels of this band are according to our calculations built upon the intrinsic configurations that apart the main $\frac{5}{2}[\mathbf{523}]$ component contains nonneglible contribution of the $\frac{5}{2}[512]$ state.

The $\frac{1}{2}[\mathbf{521}]$ *band*. Levels at 507.724$(\frac{1}{2})$, 558.211$(\frac{3}{2})$, 588.517$(\frac{5}{2})$, 705.3$(\frac{7}{2})$, 759.8$(\frac{9}{2})$, and 938.7 keV$(\frac{11}{2})$.

The newly observed level at 938.7 keV is proposed as the $\frac{11}{2}$ member of this band. The spectroscopic factors observed agree qualitatively with the model calculations for both (d,p) and $(\mathbf{d},t)$ reactions. The lowest three levels of this band are strongly populated by primary γ rays [11,12] and strongly depopulated by secondary γ rays in the (n,γ) experiments (see Table V). The resulting band parameters (A, a) are pre-

TABLE V. Gamma–decay of levels in ^{159}Gd observed in the (n,γ) reaction. Several transitions reported in the β^- decay of ^{159}Eu [10] are included. E_i, J_i^π and E_f, J_f^π denote the energy, spin and parity of the initial and final level, respectively. E_γ indicates the gamma-ray energy. Gamma-ray intensities I_γ are given per 100 neutrons captured or per 100 β^- decay, the latter quantities are presented in parenthesis.

E_i (keV)	J_i^π	E_f (keV)	J_f^π	E_γ (keV)	I_γ	E_i (keV)	J_i^π	E_f (keV)	J_f^π	E_γ (keV)	I_γ
50.627	$\frac{5}{2}^-$	0.0	$\frac{3}{2}^-$	50.7[a]		858.51	$\frac{3}{2}^+$	0.0	$\frac{3}{2}^-$	858.39	0.8
67.829	$\frac{5}{2}^+$	0.0	$\frac{3}{2}^-$	67.8[a,c]	(19.2)			50.627	$\frac{5}{2}^-$	807.60	0.4
		50.627	$\frac{5}{2}^-$	17.1[a]	(1.6)			67.829	$\frac{5}{2}^+$	790.90	1.5
118.686	$\frac{7}{2}^+$	50.627	$\frac{5}{2}^-$	67.8[a,c]	(19.2)			118.686	$\frac{7}{2}^+$	739.843	0.7
		67.829	$\frac{5}{2}^+$	51.0[a]		872.64	$\frac{5}{2}^-$	0.0	$\frac{3}{2}^-$	871.4[a]	(0.21)
121.899	$\frac{7}{2}^-$	0.0	$\frac{3}{2}^-$	121.9[a]	(0.4)			67.829	$\frac{5}{2}^+$	804.739[b]	0.7
		50.627	$\frac{5}{2}^-$	71.4[a]	(1.1)			118.686	$\frac{7}{2}^+$	754.03[b]	0.3
146.316	$\frac{5}{2}^-$	0.0	$\frac{3}{2}^-$	146.324[b]	1.4			146.316	$\frac{5}{2}^-$	726.47[b]	0.20
		50.627	$\frac{5}{2}^-$	95.685[b]	2.6			227.412	$\frac{7}{2}^-$	645.7[a]	(0.4)
		67.829	$\frac{5}{2}^+$	78.6[a]	(9.1)	880.63	$\frac{1}{2}^+,\frac{5}{2}^+$	67.829	$\frac{5}{2}^+$	813.12	0.2
185.0	$\frac{9}{2}^+$	67.829	$\frac{5}{2}^+$	118.2[a]				118.686	$\frac{7}{2}^+$	763.1[a,c]	(0.3)
212.6	$\frac{9}{2}^-$	121.899	$\frac{7}{2}^-$	90.4[a]	(0.6)						
227.412	$\frac{7}{2}^-$	0.0	$\frac{3}{2}^-$	227.5[b]	(1.6)						
		50.627	$\frac{5}{2}^-$	176.9[b]	(1.3)						
		67.829	$\frac{5}{2}^+$	159.547[b]	0.3	948.35	$\frac{7}{2}^-$	67.829	$\frac{5}{2}^+$	880.8[a]	(0.3)
		118.686	$\frac{7}{2}^+$	108.8[a]	(0.28)			118.686	$\frac{7}{2}^+$	829.7[a]	(0.6)
		121.93	$\frac{7}{2}^-$	105.5[a]	(0.7)			185.0	$\frac{9}{2}^+$	763.1[a,c]	(0.3)
		146.316	$\frac{5}{2}^-$	80.4[a]	(1.2)			227.42	$\frac{7}{2}^-$	720.9[a]	(0.16)
330.479	$\frac{9}{2}^-$	146.316	$\frac{5}{2}^-$	184.163	0.4	974.29	$\frac{1}{2}^+$	0.0	$\frac{3}{2}^-$	974.72	0.5
		227.41	$\frac{7}{2}^-$	102.5[a]	(0.7)			507.724	$\frac{1}{2}^-$	466.618[c]	1.4
507.724	$\frac{1}{2}^-$	0.0	$\frac{3}{2}^-$	507.727	5.2			558.211	$\frac{3}{2}^-$	416.09	0.2
558.211	$\frac{3}{2}^-$	0.0	$\frac{3}{2}^-$	558.195	2.7	1001.62	$\frac{3}{2}^+$	0.0	$\frac{3}{2}^-$	1001.61	0.7
		50.627	$\frac{5}{2}^-$	507.639	3.7			50.627	$\frac{5}{2}^-$	951.06	0.3
588.517	$\frac{5}{2}^-$	0.0	$\frac{3}{2}^-$	588.54[b,c]	0.20	1061.70	$\frac{1}{2}^-$	0.0	$\frac{3}{2}^-$	1061.63[b]	1.6
		50.627	$\frac{5}{2}^-$	537.86	1.4			146.316	$\frac{5}{2}^-$	915.7[a]	(0.16)
		121.93	$\frac{7}{2}^-$	466.618[c]	1.4	1079.39	$\frac{1}{2}^-$	50.627	$\frac{5}{2}^-$	1028.62	1.1
601.977	$\frac{3}{2}^+$	0.0	$\frac{3}{2}^-$	601.969[b]	4.3			146.316	$\frac{5}{2}^-$	933.08	1.2
		50.627	$\frac{5}{2}^-$	551.385[b]	2.1	1082.54	$\frac{3}{2}^-$	0.0	$\frac{3}{2}^-$	1082.37	0.5
		67.829	$\frac{5}{2}^+$	534.12	0.3			67.829	$\frac{5}{2}^+$	1015.02[b]	0.7
633.60	$\frac{7}{2}^+$	50.627	$\frac{5}{2}^-$	582.85	0.20			118.686	$\frac{7}{2}^+$	963.85[c]	1.2
646.697	$\frac{5}{2}^+$	0.0	$\frac{3}{2}^-$	646.75[b]	1.3			146.316	$\frac{5}{2}^-$	936.1[a]	(0.29)
		50.627	$\frac{5}{2}^-$	596.066[b]	0.8			507.724	$\frac{1}{2}^-$	575.5[a]	(0.26)
		121.93	$\frac{7}{2}^-$	524.77	0.9	1110.25	$\frac{3}{2}^-$	67.829	$\frac{5}{2}^+$	1043.7[a]	(0.5)
								146.316	$\frac{5}{2}^-$	963.85[c]	1.2
710.38	$\frac{7}{2}^+$	50.627	$\frac{5}{2}^-$	659.26[b]	0.3	1129.19	$\frac{1}{2}^+$	0.0	$\frac{3}{2}^-$	1128.47[b]	1.1
		121.899	$\frac{7}{2}^-$	588.54[b,c]	0.20			50.627	$\frac{5}{2}^-$	1078.57[b]	1.0
		212.6	$\frac{9}{2}^-$	498.2[a]	(0.3)	1139.84	$\frac{1}{2}^-$	0.0	$\frac{3}{2}^-$	1139.90	1.9
732.87	$\frac{5}{2}^-,\frac{7}{2}^-$	67.829	$\frac{5}{2}^+$	665.04[b]	0.20			781.556	$\frac{1}{2}^+$	358.264	0.2
		118.686	$\frac{7}{2}^+$	613.4[a]	(1.3)	1145.60	$\frac{3}{2}^-$	50.627	$\frac{5}{2}^-$	1095.18[b]	0.8
744.378	$\frac{3}{2}^+$	0.0	$\frac{3}{2}^-$	744.375[b]	0.6			781.556	$\frac{1}{2}^+$	364.029	0.3
		50.627	$\frac{5}{2}^-$	693.73[b]	0.5	1159.90	$\frac{5}{2}^+$	0.0	$\frac{3}{2}^-$	1159.4[a]	(0.06)
		67.829	$\frac{5}{2}^+$	676.512[b]	1.7			50.627	$\frac{5}{2}^-$	1109.0[a]	(0.26)

TABLE V. (*Continued.*)

E_i (keV)	J_i^π	E_f (keV)	J_f^π	E_γ (keV)	I_γ	E_i (keV)	J_i^π	E_f (keV)	J_f^π	E_γ (keV)	I_γ
781.556	$\frac{1}{2}^+$	0.0	$\frac{3}{2}^-$	781.56	1.0			118.686	$\frac{7}{2}^-$	1038.2[a]	(0.19)
		67.829	$\frac{5}{2}^+$	713.649	2.0	1394.45	$\frac{1}{2}^+\frac{3}{2}^+$	872.64	$\frac{5}{2}^-$	521.4[a]	(0.17)
		507.724	$\frac{1}{2}^-$	273.856	0.20	1400.2	$\frac{1}{2}^-\frac{3}{2}^-$	50.627	$\frac{5}{2}^-$	1350.8[a]	(0.12)
800.45	$\frac{5}{2}^+$	0.0	$\frac{3}{2}^-$	800.39	0.20	1431.0	$\frac{1}{2}^+\frac{3}{2}^+$	0.0	$\frac{3}{2}^-$	1430.8[b]	2.0
		67.829	$\frac{5}{2}^+$	732.68[b]	0.20	1468.31	$\frac{3}{2}^+$	0.0	$\frac{3}{2}^-$	1468.6[a]	(0.29)
		118.686	$\frac{7}{2}^+$	681.71[b]	0.7	1520.86	$\frac{1}{2}^-$	0.0	$\frac{3}{2}^-$	1520.0[a]	(0.7)
		121.93	$\frac{7}{2}^-$	678.53	0.3						
818.89	$\frac{5}{2}^+$	50.627	$\frac{5}{2}^-$	768.15	0.3						
		67.829	$\frac{5}{2}^+$	751.23	0.5						
		118.686	$\frac{7}{2}^+$	700.163	1.0						
		185.0	$\frac{9}{2}^+$	633.78	0.4						
		646.697	$\frac{5}{2}^+$	172.368	0.3						

[a]Observed in β^- decay *only*. Transition energies and intensities (given in parenthesis) are taken from Ref. [10].
[b]Observed in β^- decay *also*. Transition energies and intensities are taken from Table I.
[c]Multiply placed (doublet).

cisely conserved with increasing spin. The level spacing pattern observed (with decoupling parameter $a=0.46$) is very closely reproduced in neighboring odd-A nuclei from ^{153}Gd through ^{161}Gd and ^{161}Dy and ^{163}Er [52–56]. The recent suggestion to rearrange the level spacing in this band known in ^{157}Gd [54] by lowering the $\frac{3}{2}$ level and yielding $a=-0.13$ [16] is not supported in our analysis.

The $\frac{11}{2}$[**505**] *band*. Level at 684.16 keV$\left(\frac{11}{2}\right)$.

The differential cross sections of the transfer reactions populating this level suggest the transferred momentum is $l=4$ or $l=5$ in the (d,p) reaction, and the total angular momentum $j=\frac{9}{2}^+$ or $\frac{11}{2}^-$ in $(\mathbf{d},t)$ reaction. Our choice is based on the previous identification of this state in ^{159}Gd at 681 keV [1]. The corresponding experimental spectroscopic

TABLE VI. Evolution of the experimental effective rotational parameters A and decoupling parameters a of rotational bands in ^{159}Gd. Corresponding values obtained in the model calculation with the Coriolis interaction included (see Sec. VI) and the pure Nilsson a values are given in the two rightmost columns.

Band	Energy	A values (in keV) and a-parameters							
$K[Nn_z\Lambda]$	(keV)	$\frac{1}{2}-3/2(-5/2)$	$3/2-5/2(-7/2)$	$5/2-7/2(-9/2)$	$7/2-9/2(-11/2)$	$9/2-11/2$	$11/2-13/2$	Coriolis	Nilsson
$\frac{3}{2}$[521]	0.0		10.12	10.18	10.10	10.19		12.1	
$\frac{5}{2}$[642]	67.829			7.27	7.43	8.05	7.59	14.9	
$\frac{5}{2}$[523]	146.316			11.58	11.45	11.45		12.3	
$\frac{1}{2}$[521]	507.724	11.42(0.47)	11.31(0.47)	11.35(0.46)	11.2(0.45)			11.6(0.37)	(0.37)
$\frac{3}{2}$[651]	601.977		8.96					8.8	
$\frac{7}{2}$[633]	633.60				14.16	13.87		11.5	
$\frac{3}{2}$[402]	744.378		11.22	11.02				11.6	
$\frac{1}{2}$[660]	781.556	8.85(1.91)						7.0(3.50)	(5.05)
$\frac{5}{2}$[512]	872.64			10.85	10.55			10.6	
$\frac{1}{2}$[400]	974.29	10.22(−0.14)	10.15(−0.14)	10.44(−0.16)				9.6(−0.35)	(−0.35)
$\frac{3}{2}$[532]	1110.25		13.64	11.71	14.04			11.2	
$\frac{7}{2}$[514]	1134.7				7.66			6.9	
$\frac{1}{2}$[530]	1139.84	11.80(−0.83)	14.24(−0.49)	11.30(−0.36)				9.9(−0.45)	(1.24)
$\frac{1}{2}$[510]	1579.6	13.03(−0.38)	12.76(−0.41)					10.1(-0.53)	(−5.90)
$\frac{3}{2}$[512]	1637.8	12.88						9.2	
$\frac{1}{2}$[651]	1983.3	11.86(−0.44)						11.8(−0.44)	(1.58)

factors confirm the proposed identification of this level as a hole state in ^{159}Gd, in agreement with the systematics of this orbital in neighboring odd-A nuclei.

The $\frac{5}{2}$[**512**] *band*. Levels at 872.64($\frac{5}{2}$), 948.35($\frac{7}{2}$) and 1043.2 keV($\frac{9}{2}$).

The previous identification of this band in ^{159}Gd [1] is confirmed. The level at 1186 keV, previously proposed as the $\frac{11}{2}^-$ member of this band [1], was not observed in our experiments. While the $\frac{5}{2}$ level is not observed in the transfer reaction experiments, the $\frac{7}{2}$ level exhibits a large spectroscopic factor in the (d,p) reaction. This is explained, at least partially, by the model prediction. According to our calculations the intrinsic structure of this band is regarded as a mixture of the $\frac{5}{2}$[512] and $\frac{5}{2}$[523] Nilsson configurations. This band is well reproduced in the neighboring nuclei ^{161}Gd and ^{161}Dy [55]. In ^{157}Gd merely the $\frac{7}{2}$ member has been identified [54]

The $\frac{3}{2}$[**532**] *band*. Levels at 1110.25($\frac{3}{2}$), 1178.6($\frac{5}{2}$), 1239.4($\frac{7}{2}$), and 1365.9 keV($\frac{9}{2}$).

The previous identification of this band in ^{159}Gd [1] is confirmed including the newly observed $\frac{9}{2}^-$ level at 1365.9 keV. The observed spectroscopic factors are in agreement with the interpretation of this band. Our calculations show that due to the Coriolis interaction the levels of this band should be interpreted as mixtures of the $\frac{3}{2}$[532] and $\frac{1}{2}$[530] configurations. We find that admixtures of the $\frac{1}{2}$[530] configuration into the experimentally observed levels are typically 25–50%. The $\frac{7}{2}$ state is, within the model used, interpreted as an almost ideal superposition of both configurations. Such an interpretation explains the lowering of the $\frac{7}{2}$ level and consequently the change in the moment of inertia within this band. This band is well reproduced in ^{157}Gd [16] and ^{155}Gd [53]. The systematics of this orbital in adjacent odd-*A* nuclei supports the proposed identification.

The $\frac{1}{2}$[**530**] *band*. Levels at 1139.84($\frac{1}{2}$), 1145.60($\frac{3}{2}$), 1253.1($\frac{5}{2}$), 1303.4($\frac{7}{2}$), and 1442.8 keV($\frac{9}{2}$).

The $\frac{3}{2}$ and $\frac{5}{2}$ levels previously assigned to this band [1] are confirmed in this work. Additional $\frac{7}{2}$, $\frac{9}{2}$, and $\frac{11}{2}$ levels reported at 1238, 1301, and 1390 keV [1] are not observed in our experiments. Instead, we propose to assign three newly measured levels to this band as indicated. The spectroscopic factors measured for these three levels are in reasonable agreement with the model calculations. As mentioned earlier (see $\frac{3}{2}$[532] band), our calculations indicate strong Coriolis coupling of the $\frac{1}{2}$[530] and $\frac{3}{2}$[532] configurations. The observed rotational band parameters ($A=12.9$ keV, $a=-0.56$) agree well with the values recently reported for ^{157}Gd ($A=10.5$ keV, $a=-0.51$) [16]. These values differ from the rotational band parameters previously reported for ^{157}Gd ($A=5.6$ keV, $a=-0.10$) [54], ^{161}Dy ($A\approx 9$ keV, $a\approx -1.5$ [14]), ^{155}Gd ($A\approx 13$ keV, $a\approx -1.0$ [15]), and ^{163}Er ($A=8.9$ keV, $a=0.53$ [56]).

The $\frac{7}{2}$[**514**] *band*. Levels at 1134.7($\frac{7}{2}$) and 1203.5 keV($\frac{9}{2}$).

We propose this identification based on the spectroscopic factors observed in the transfer reactions which are qualitatively well reproduced by the model predictions and the excitation energy expected for this orbital in this region [18]. The intrinsic configuration on which this band is built upon is interpreted in the model calculations as a state composed of the $\frac{7}{2}$[514] component with a significant contribution of the $\frac{7}{2}$[503] Nilsson configuration with non-negligible quasiparticle-octupole-phonon admixtures. This orbital has been previously reported only in ^{153}Gd at 636 keV [52].

The $\frac{1}{2}$[**510**] *band*. Levels at 1579.6($\frac{1}{2}$), 1603.30($\frac{3}{2}$), 1693.5 keV($\frac{5}{2}$), and 1728.3 keV($\frac{7}{2}$).

The previous assignment of the $\frac{3}{2}$ level at 1603 keV to this band [1] is confirmed. The $\frac{5}{2}$ and $\frac{7}{2}$ levels at 1638 and 1751 keV [1] are not observed in our experiments. We propose three newly observed levels to this band including the band head. The spectroscopic factors observed for these levels and the rotational band parameters derived from our experiments are in good agreement with the model values. Our rotational band parameters ($A=12.9$ keV, $a=-0.39$) agree with those reported for ^{163}Er ($A=12.3$ keV, $a=-0.38$) [56] but differ from those reported for ^{155}Gd ($A=15.3$ keV, $a=0.11$), ^{161}Gd ($A=11.0$ keV, $a=-0.18$), and ^{163}Dy ($A=11.7$ keV, $a=-0.04$) [53,55,56]. Our QPM calculations indicate that the corresponing intrinsic configuration has a complex structure.

The $\frac{9}{2}$[**514**] *band*. Level at 1622.3 keV($\frac{11}{2}$).

Similarly to the $\frac{11}{2}$ level at 684.16 keV discussed earlier (see $\frac{11}{2}$[505] band), the differential cross section of the $(\mathbf{d},t)$ reaction that describes the population of this level indicates either $j=\frac{9}{2}^+$ or $\frac{11}{2}^-$. Our tentative interpretation is based upon the large experimental spectroscopic factor. This orbital has not been previously reported in neighboring odd-*A* nuclei [50].

The $\frac{3}{2}$[**512**] *band*. Levels at 1637.8($\frac{3}{2}$), 1702.1($\frac{5}{2}$), and 1809.2($\frac{7}{2}$).

These levels are tentatively assigned to this band based on the large spectroscopic factors observed in the (d,p) reaction. This identification is supported by their excitation energies which are close to the $\frac{1}{2}$[510] band [57], and also by our QPM calculations predicting the corresponding intrinsic state with non-negligible quasiparticle-phonon admixtures in the suitable energy region. The level spacing and the rotational band parameter, $A=13.0$ keV, derived from the experimental data are in reasonable agreement with the level spacing and band parameters reported for this band in ^{161}Dy and ^{153}Gd [52,55]. The $\frac{3}{2}$[512] orbital appears very close to the $\frac{1}{2}$[510] orbital also in ^{153}Gd [52].

The $\frac{1}{2}$[**770**] *band*. Levels at 1997.3($\frac{3}{2}$) and 2058.0($\frac{7}{2}$).

We tentatively propose these two levels as candidates of rotational levels to this band. The proposed identification is based on the high excitacion energy and the large spectroscopic factors observed in the (d,p) reaction which correspond to the model predictions, see also Refs. [57] and [58]. The $\frac{1}{2}$ and $\frac{5}{2}$ levels of this band are expected to be only weakly populated [58].

C. Rotational bands with positive parity

The $\frac{5}{2}$[**642**] *band*. Levels at 67.829($\frac{5}{2}$), 118.686($\frac{7}{2}$), 185.0($\frac{9}{2}$), 273.9($\frac{11}{2}$), and 372.7 keV($\frac{13}{2}$).

The previous identification of this band in ^{159}Gd [1] is confirmed. Coriolis band mixing calculations predict that

these experimentally observed states should be considered as the band built upon the $\frac{5}{2}$[642] configuration with admixtures of the $\frac{3}{2}$[651] and $\frac{7}{2}$[633] Nilsson orbitals (each typically with 10%–20%). The spectroscopic factors observed for these levels agree with the calculated values. Together with the $\frac{3}{2}$[651] orbital, the $\frac{5}{2}$[642] orbital appears as a particle state in ^{153,155}Gd, and as a hole state in ^{157,159,161}Gd. The $\frac{5}{2}$[642] orbital becomes the ground state in ^{161}Dy. This rotational band is well reproduced in ^{157}Gd [16] and, to a lesser extent, also in ^{161}Dy [55] and ^{155}Gd [53].

The $\frac{3}{2}$[**651**] *band*. Levels at 601.977$(\frac{3}{2})$, 646.697$(\frac{5}{2})$, and 710.38 keV$(\frac{7}{2})$.

The previous identification of this band in ^{159}Gd [1] is confirmed including the newly observed $\frac{7}{2}$ level at 710.38 keV which is reported in γ-γ coincidences in β^- decay of ^{159}Eu [10] and confirmed by our secondary γ-ray data (Table V). Coriolis band mixing calculations indicate that the observed levels should be considered as mixtures of the main component with the $\frac{1}{2}$[660], $\frac{5}{2}$[642], and $\frac{7}{2}$[633] Nilsson configurations; these admixtures depend on the level spin and their sum is 20–40%. These effects can, at least qualitatively, account for their irregular and weak population in the transfer reactions. This rotational band is well reproduced in ^{161}Dy [14] in contrast to the irregular and inverted level sequence reported for this band in ^{155}Gd [15] and ^{157}Gd [16,59].

The $\frac{7}{2}$[**633**] *band*. Levels at 633.60$(\frac{7}{2})$ and 1093.0 keV$(\frac{13}{2})$.

These newly observed levels are proposed for this band based on their spectroscopic factors and excitation energies. The final spin assignments (Table IV) are selected according to the model values of spectroscopic factors. The two experimentally observed levels appear due to the Coriolis interaction as states that, aside the main $\frac{7}{2}$[633] component, contain also non-negligible admixtures of the $\frac{1}{2}$[660], $\frac{3}{2}$[651], and $\frac{5}{2}$[642] Nilsson configurations (see $\frac{3}{2}$[651] band). The $\frac{7}{2}$[633] orbital has been reported at 1231 MeV in ^{157}Gd [59], at 510 keV in ^{161}Gd [50], and at 772 keV in ^{161}Dy [50]. A $\frac{13}{2}$ level at 1146 keV has been assigned to this band in ^{155}Gd [15].

The $\frac{3}{2}$[**402**] *band*. Levels at 744.378$(\frac{3}{2})$, 800.45$(\frac{5}{2})$, and 876.5 keV$(\frac{7}{2})$.

The $\frac{3}{2}$ and $\frac{5}{2}$ levels previously assigned to this band [1] are confirmed. We propose the newly observed level at 876.5 keV as the $\frac{7}{2}$ member of this band based on its excitation energy and spectroscopic strength. The $\frac{3}{2}$ member exhibits the largest experimental spectroscopic factor in the $(\mathbf{d},t)$ reaction. The lowest two levels of this band are strongly populated [11,12] and depopulated in the (n,γ) reactions (Table V). The spectroscopic factors observed for the three levels are in agreement with the model predictions.

The $\frac{1}{2}$[**660**] *band*. Levels at 781.556$(\frac{1}{2})$, 818.89$(\frac{5}{2})$, and 858.51 keV$(\frac{3}{2})$.

The lowest two levels previously assigned to this band [1] are confirmed in our data. The $\frac{3}{2}^+$, $\frac{7}{2}^+$, and $\frac{13}{2}^+$ levels at 1001, 1282, and 1056 keV [1,9] are not observed in our experiments. We propose the newly observed level at 858.51 keV as the $\frac{3}{2}^+$ state of this band based on the spectroscopic factors and the resulting level ordering. In our model calculations, the levels of this band appear as mixtures of several quasiparticle configurations (see $\frac{3}{2}$[651] band). This rotational band is well reproduced in ^{155}Gd [15] and with a reversed level ordering in ^{161}Dy.

The $\frac{1}{2}$[**400**] *band*. Levels at 974.29$(\frac{1}{2})$, 1001.62$(\frac{3}{2})$, 1059.6$(\frac{5}{2})$, 1120.3$(\frac{7}{2})$, and 1229.3$(\frac{9}{2})$.

The $\frac{1}{2}$ level was previously assigned to this band [1]. A previously reported $\frac{3}{2}$ level at 1061 keV [1] is now proposed as the $\frac{5}{2}$ member of this band based on precise spin assignment deduced from the $(\mathbf{d},t)$ reaction. Additionally, the $\frac{7}{2}$ and $\frac{9}{2}$ states are identified. These assignments are based on the observed spectroscopic factors and the resulting rotational band parameters. This rotational band is well reproduced in ^{155}Gd [15] and ^{157}Gd [16] and, with a reversed ordering, in ^{161}Dy [14,55].

The $\frac{7}{2}$[**404**] *band*. Levels at 1532.4 keV$(\frac{7}{2})$ and 1631.4 keV$(\frac{9}{2})$.

The level at 1960 keV previously assigned as the $\frac{7}{2}$ member of this band [1] is not observed in our experiments. Our interpretation is based on the spins, energies and spectroscopic factors observed, which agree with our model values and with the values presented in Refs. [57] and [58]. The band head of the $\frac{7}{2}$[404] rotational band has been observed at 1297 keV in ^{155}Gd [15], at 1416 keV in ^{161}Dy [55], and at 1825 keV in ^{157}Gd [54]. Rather large quasiparticle-quadrupole-phonon admixtures into the intrinsic state the band is built upon are predicted in our QPM calculations.

The $\frac{5}{2}$[**402**] *band*. Level at 1964.6 keV$(\frac{5}{2})$.

We tentatively assign the level at 1964.6 keV as the $\frac{5}{2}$ state of this band based on the excitation energy and the large spectroscopic factor observed in the $(\mathbf{d},t)$ reaction which agree with the model values and the values reported in Refs. [57] and [58].

The $\frac{1}{2}$[**651**] *band*. Levels at 1983.3$(\frac{1}{2})$, 2003.2$(\frac{3}{2})$, and 2088.1 keV$(\frac{5}{2})$.

The group of levels around 2 MeV previously assigned to this band [1] is confirmed. The excitation energies and spectroscopic factors observed for these levels in the (d,p) reaction reasonably agree with the model values (see also Refs. [57] and [58]). This band is reported with a similar level ordering ($E_{J=1/2}=1490$ keV, $A=5.7$ keV, $a=1.30$) in ^{161}Dy [55] and with a different level spacing ($E_{J=1/2}=1434$ keV, $A=7.3$ keV, $a=-0.5$) in ^{155}Gd [15]. In ^{153}Gd [52], this orbital is reported with the bandhead at 731 keV and with an irregular level ordering.

D. Rotational band parameters

The effective rotational parameters A and decoupling parameters a (for $K=\frac{1}{2}$) for the rotational bands were calculated from two or three (for $K=\frac{1}{2}$) adjacent levels using the expression

$$E = E_0 + A[J(J+1) + (-1)^{J+1/2}a(J+1/2)]. \quad (4)$$

The band parameters deduced with this equation are listed in Table VI. The experimental values obtained reflect the regu-

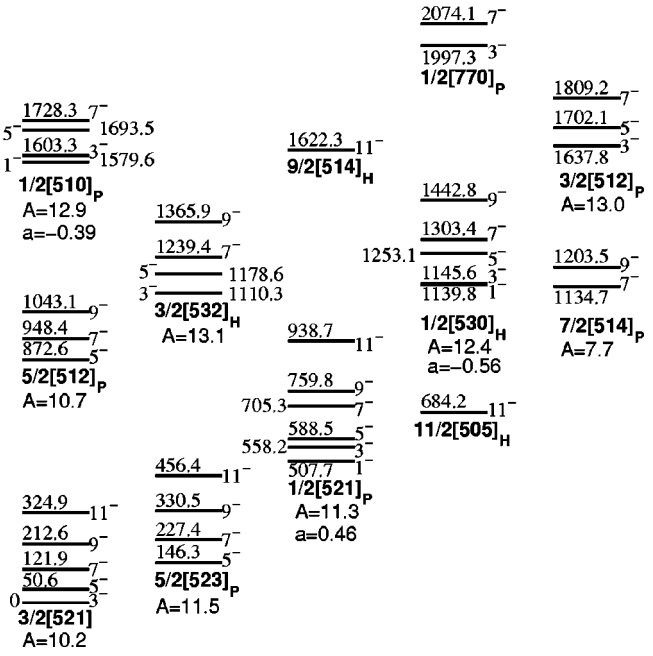

FIG. 8. Negative-parity rotational bands in ^{159}Gd. Energy and spin (in $\hbar/2$ units) of levels as well as band assignments in terms of Nilsson states are given. Also, the experimentally observed rotational band parameters A (in kilo-electron-volts) and a are indicated. The dominant character of orbitals, either hole (H) or particle (P), is denoted as subindex.

larity of the bands. The corresponding values deduced from the model calculations with Coriolis interaction included (see Sec. VI) and the Nilsson a-values are presented in Table VI for comparison. The rotational band parameters given in Figs. 8 and 9 are arithmetic averages of the corresponding values given in Table VI.

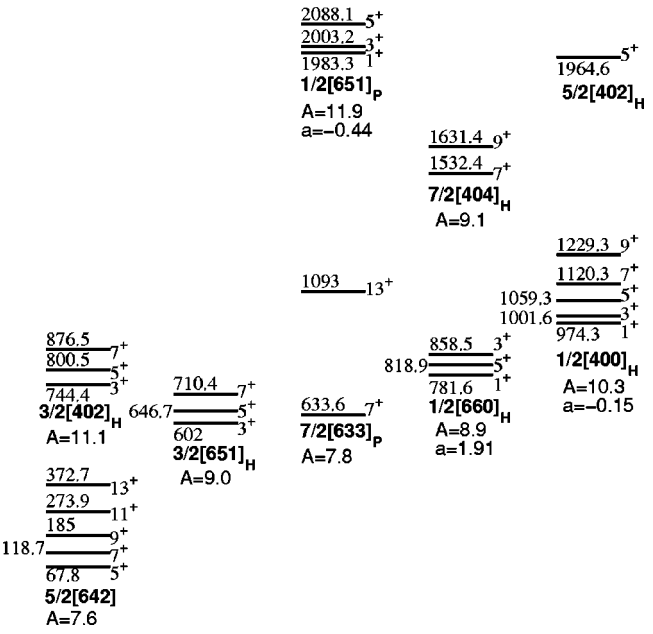

FIG. 9. Positive-parity rotational bands in ^{159}Gd (see caption of Fig. 8).

TABLE VII. Levels in ^{159}Gd proposed as candidates for quasiparticle-vibrational states. The energy predicted in QPM calculations is included; the dominant configuration and its percentage is given.

E_{exp}(keV)	E_{th}(keV)	J^{π}	Configuration
1128.73	1850	$1/2^{+}$	$3/2[521]\{Q_{31}+Q_{32}\}95\%$
1159.90	1879	$5/2^{+}$	$3/2[521]Q_{31}93\%$
1782.53	1785	$1/2^{-}$	$5/2[642]\{Q_{33}+Q_{32}\}64\%$

E. Comments on quasiparticle-vibrational states

Many of the low-lying levels observed in the ^{159}Gd nucleus and most of the observed secondary γ rays have been identified among low-lying states which exhibit dominant quasiparticle characters. Nevertheless, the possibility that collective vibrations are in some degree present in experimentally observed states cannot be excluded [29] especially at higher energies; for ^{155}Gd see, e.g., Ref. [60].

From the spectroscopic results obtained in this work, we make the following tentative suggestions regarding possible candidates for quasiparticle-vibrational states in ^{159}Gd. The observed γ decays of levels at 1128.73 and 1159.90 keV to the ground state rotational band (see Table V) and the relatively strong population of these levels by primary γ rays [11,12] suggest quasiparticle-vibrational admixtures to these levels. The latter level is observed in the $(\mathbf{d},t)$ reaction with a rather large spectroscopic factor. Both these levels would correspond to the coupling of the octupole 1^{-} phonon (the lowest vibration in ^{158}Gd observed at 977 keV [50]) to the ground state $\frac{3}{2}$[521] orbital in ^{159}Gd yielding a pair of $\frac{1}{2}^{+}$ and $\frac{5}{2}^{+}$ states. However, the QPM calculations place these levels at higher energies. The $\frac{1}{2}^{-}$ level observed at 1782.53 keV in the (d,p) reaction is suggested as a possible candidate of a quasiparticle-vibrational state based on its relatively strong population by the primary γ rays [12], excitation energy and spectroscopic factor measured. This identification agrees with model calculations which predict a complex state with dominant $\frac{5}{2}[642]\{Q_{33}+Q_{32}\}$ components in this energy region. These levels, as candidates for quasiparticle-vibrational states, are listed in Table VII where we include the proposed configurations and corresponding excitation energies derived from the model calculations (Sec. VI).

V. SYSTEMATICS OF ADJACENT NUCLEI

An essential result of nuclear spectroscopic studies is the establishment of the systematic behaviour of nuclear excitations. Single particle excitations identified with their Nilsson assignments represent the basis for the shell model interpretation of deformed nuclei. The systematic variation of experimental band head energies of predominantly single particle bands in the odd-mass Gd isotopes ($Z=64$) is displayed in Fig. 10. Excitations with dominant particle and hole character are plotted with positive and negative energies, respectively. The level energies are taken from the following references: ^{153}Gd [52], ^{155}Gd [15,53], ^{157}Gd [54,59], and ^{161}Gd

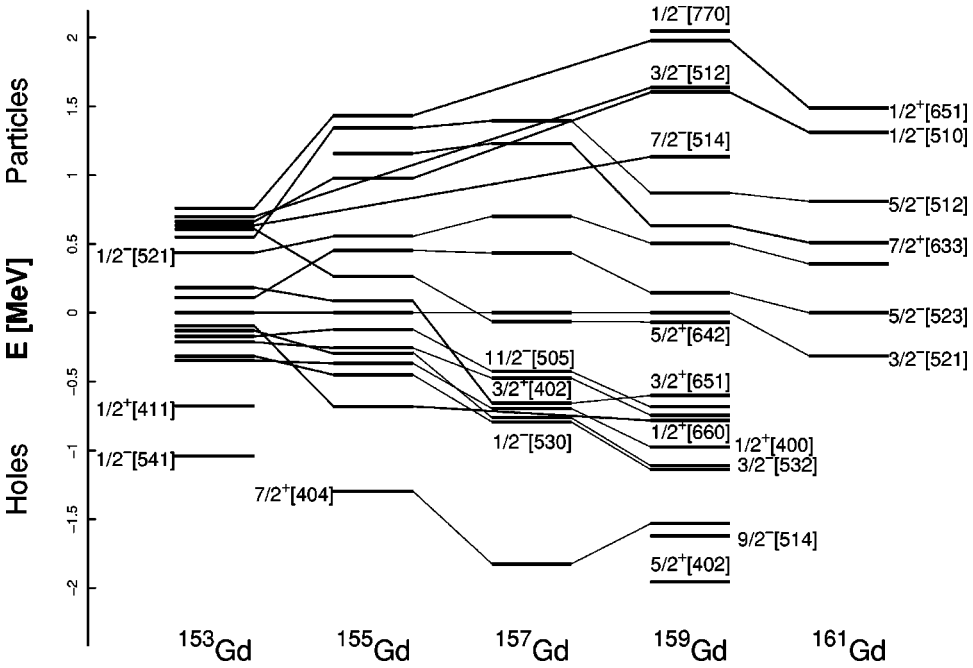

FIG. 10. Systematics of quasiparticle states for the Gd isotopes.

[55]. Figure 10 appears very similar to a corresponding plot of single particle excitations in the Dy isotopes [14]. Even details are reproduced, for instance, the increase and decrease of the excitation energy of the $\frac{1}{2}$[521], $\frac{5}{2}$[512], and $\frac{5}{2}$[523] particle states with the neutron number. This systematic information should help to perform precise calculations for deformed nuclei.

Similarly, the systematics of the band head energies of single particle excitations across odd-mass nuclei with $N=95$ is shown in Fig. 11. The level energies are taken from the following references: ^{157}Sm [50], ^{161}Dy [14,55], ^{163}Er [56], and ^{165}Yb [50,61].

VI. MODEL CALCULATION

A. Formulation

The low-lying states in odd-A deformed nuclei can be satisfactorily described within the adiabatic approximation of the separation of intrinsic and rotational motion. In order to describe the intrinsic nuclear motion and vibrational admixtures to quasiparticle states in particular, we adopt the QPM based on the assumption that the experimental data reflect the fragmentation of quasiparticle and quasiparticle-phonon states [29]. To this end, we assume an axially symmetric average nuclear field in which nucleons move and interact

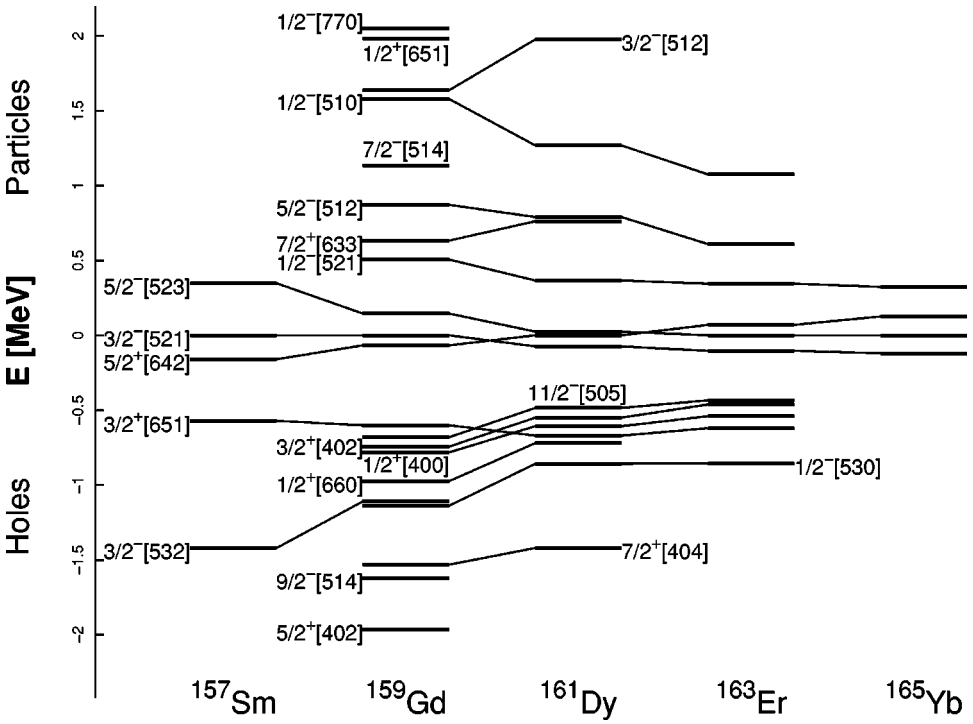

FIG. 11. Systematics of quasiparticle states for the $N=95$ isotones.

through pairing as well as residual interactions. The short-range pairing of protons and neutrons is solved in the constant pairing gap approximation. The long-range separable multipole-multipole residual interactions between nucleons are treated microscopically within the random phase approximation (RPA). The rotation of the whole system in the laboratory frame is taken into account using the standard quasiparticle-rotor model.

Assuming that the odd proton and neutron quasiparticles move independently, we first generate the system of quasiparticle states for the even-even core in the average Nilsson potential. We adopt the potential parameters as recommended in Ref. [29] and the quadrupole and hexadecapole deformation paremeters $\delta=0.25$ and $\beta_{40}=0.08$. All proton and neutron shells with the main quatum numbers $N=2-7$ are included in the calculation. Pairing gaps are taken as $\Delta_p=0.87$ MeV and $\Delta_n=0.75$ MeV for protons and neutrons, respectively. Fermi levels are approximated by the model particle energies of the ground state in the $A=159$ nuclei ^{159}Gd and ^{159}Tb. In a next step, phonon excitations of the even–even core are evaluated by solving the RPA equation. We restrict ourselves to quadrupole and octupole charge independent excitations. The experimental energies of quadrupole and octupole one-phonon states in the even-even neighboring core ^{158}Gd are used to deduce the strengths of the residual multipole-multipole forces. Their values are namely $E_{1^-}=977$ keV, $E_\gamma=1187$ keV, and $E_\beta=1196$ keV for the band head energies of the octupole 1^- and quadrupole γ and β bands in the ^{158}Gd core, respectively [50]. For the collective modes with vanishing spin projection onto the intrinsic symmetry axis, we obtained, for example, the following values of the strength of the residual multipole-multipole interactions: $\kappa_{20}=1.67$ keV and $\kappa_{30}=0.0582$ keV. Finally, the quasiparticle-phonon interaction is analyzed and the QPM secular equation is solved. At this step, the quasiparticle energies are adjusted in order to improve the agreement between experimental and model energies. The resultant intrinsic wave functions contain both quasiparticle and quasiparticle-phonon components exhibiting in such a way vibrational admixtures into specific states.

States of rotational bands and their structures are calculated in the quasiparticle-rotor approach assuming the odd valence neutron is coupled to the rigid rotator. The Coriolis band mixing calculation of the states is performed in a standard manner. Our model space includes 14 negative parity bands and 9 positive parity bands in ^{159}Gd. In our calculations, the intrinsic energy parameters, inertia parameters, and also decoupling parameters of experimentally observed bands are varied to achieve the best agreement with experiment. Due to the Coriolis interaction, resultant wave functions of a given spin and parity can be written as a linear combination of the intrinsic quasiparticle states with possible quasiparticle-phonon admixtures.

We use the Nilsson model asymptotic quantum numbers $K[Nn_n\Lambda]$ as labels of individual quasiparticle states. Phonon states are listed as $Q_{\lambda\mu}$ where λ is the multipolarity of the phonon and μ is its projection on the intrinsic symmetry axis. The basis of the quasiparticle-phonon states are written as $K^\pi[Nn_z\Lambda]Q_{\lambda\mu}$. Experimentally observed levels are usually assigned by its dominant quasiparticle component.

B. Results and discussion

Results of our calculation on the structure of individual intrinsic states in the ^{159}Gd nucleus are presented in Table VIII. This table contains the experimental and theoretical band head energies as well as the structure of the intrinsic states up to 1.8 MeV (above 1.8 MeV many complex states with quasiparticle-vibrational components appear). The admixture of the dominant quasiparticle configuration and additional quasiparticle-phonon admixtures are indicated. The calculations carried out show that most of the low-lying ($E<1$ MeV) instrinsic states in ^{159}Gd can be understood as almost pure quasiparticle states. However, with increasing excitation energy, the model predicts more complex configurations; states with dominant vibrational components should lie preferentially above 1.8 MeV in this nucleus. These results agree with a similar description of ^{155}Gd [60]. An interesting result of our calculations is that the lowest two intrinsic states with $J^\pi=\frac{5}{2}^-$ in ^{159}Gd should be considered as combination of the $\frac{5}{2}[523]$ and $\frac{5}{2}[512]$ Nilsson states. Similarly, the lowest intrinsic state with $J^\pi=\frac{7}{2}^-$ that is assigned as the $\frac{7}{2}[514]$ state contains non-negligible contribution of the $\frac{7}{2}[503]$ Nilsson configuration. The quasiparticle-phonon approach fails to reproduce the intrinsic states with a dominant $\frac{1}{2}[770]$, $\frac{5}{2}[402]$, or $\frac{1}{2}[651]$ configuration that are identified experimentally near 2 MeV.

In the Coriolis band mixing calculations we obtained reasonable agreement between experimentally observed levels and their model counterparts. All low-lying ($E<1$ MeV) rotational bands were reproduced with discrepancies lower than 20 keV. These calculations reveal that the two near-lying rotational bands assigned as the $\frac{1}{2}[530]$ and $\frac{3}{2}[532]$ bands should be interpreted as bands built upon mixed quasiparticle configurations. Also, the states that we have assigned as members of the rotational bands built upon the $\frac{1}{2}[510]$ and $\frac{3}{2}[512]$ Nilsson orbitals should be, due to the Coriolis interaction, regarded as states with strongly mixed quasiparticle content. Similarly, we found that the experimentally observed levels that can be interpreted as members of the rotational bands built upon the $\frac{7}{2}[633]$, $\frac{5}{2}[642]$, $\frac{3}{2}[651]$, and $\frac{1}{2}[660]$ Nilsson configurations (from $i_{13/2}$) have complex structures and are strongly coupled by the Coriolis interaction. Calculated values of the moment of inertia and decoupling parameters of all rotational bands included in the Coriolis mixing analysis are given in the last column of Table VI to be compared with the experimental results obtained with the simple rotational Eq. (4).

As a final test for the model interpretation of the experimentally observed levels, we calculated the spectroscopic factors of the pickup and stripping processes. The calculated values obtained in the Coriolis band mixing calculation are summarized and compared with the experimental results in Table IX. With few discrepancies, we find that the relative values of most of the experimentally observed spectroscopic factors in a rotational band are satisfactorily reproduced by the model factors labeled by the main quantum number N from the dominant Nilsson assignment of a state. For example, experimentally observed spectroscopic factors of particle-hole structures of the lowest five rotational bands are

TABLE VIII. Structure of low-lying intrinsic states in ^{159}Gd. Experimental band head energies are compared with values obtained in QPM calculations. Percentages of the main components of the quasiparticle-phonon admixtures are given. Only components greater than 5% are included. Level energies are given in kilo-electron-volt.

J^π	E_{exp}	E_{th}	Structure $K[Nn_n\Lambda]Q_{\lambda\mu}$
$\frac{3}{2}^-$	0.0	0	$\frac{3}{2}[521]83\%$
$\frac{5}{2}^+$	67.829	89	$\frac{5}{2}[642]84\%$
$\frac{5}{2}^-$	146.316	93	$\frac{5}{2}[523]42\% + \frac{5}{2}[512]30\% + \{\frac{5}{2}[642]Q_{30}\}8\% + \{\frac{11}{2}[615]Q_{33}\}7\%$
$\frac{1}{2}^-$	507.724	497	$\frac{1}{2}[521]71\%$
$\frac{3}{2}^+$	601.977	578	$\frac{3}{2}[651]77\%$
$\frac{7}{2}^+$	633.60	672	$\frac{7}{2}[633]68\% + \{\frac{3}{2}[521]Q_{32}\}16\%$
$\frac{11}{2}^-$	684.16	695	$\frac{11}{2}[505]85\% + \{\frac{5}{2}[402]Q_{33}\}9\%$
$\frac{3}{2}^+$	744.378	755	$\frac{3}{2}[402]81\% + \{\frac{1}{2}[400]Q_{22}\}8\%$
$\frac{1}{2}^+$	781.556	799	$\frac{1}{2}[660]81\%$
$\frac{5}{2}^-$	872.64	1088	$\frac{5}{2}[512]41\% + \frac{5}{2}[523]45\%$
$\frac{1}{2}^+$	974.29	989	$\frac{1}{2}[400]70\% + \{\frac{3}{2}[402]Q_{22}\}13\% + \{\frac{3}{2}[521]Q_{31}\}7\%$
$\frac{3}{2}^-$	1110.25	1126	$\frac{3}{2}[532]73\% + \{\frac{3}{2}[402]Q_{30}\}12\%$
$\frac{7}{2}^-$	1134.7	1177	$\frac{7}{2}[514]47\% + \frac{7}{2}[503]21\% + \{\frac{13}{2}[606]Q_{33}\}12\% + \{\frac{7}{2}[633]Q_{30}\}8\%$
$\frac{1}{2}^-$	1139.84	1172	$\frac{1}{2}[530]82\% + \{\frac{1}{2}[400]Q_{30}\}6\%$
$\frac{5}{2}^+$		1186	$\frac{5}{2}[402]22\% + \{\frac{11}{2}[505]Q_{33}\}55\% + \{\frac{1}{2}[400]Q_{22}\}5\%$
$\frac{7}{2}^+$	1532.4	1526	$\frac{7}{2}[404]68\% + \{\frac{3}{2}[402]Q_{22}\}22\%$
$\frac{1}{2}^-$	1579.6	1714	$\frac{1}{2}[510]39\% + \{\frac{5}{2}[642]Q_{33}\}20\% + \{\frac{5}{2}[642]Q_{32}\}8\% + \{\frac{5}{2}[512]Q_{22}\}5\%$
$\frac{9}{2}^-$	1622.3[a]	1643	$\frac{9}{2}[514]83\% + \{\frac{3}{2}[411]Q_{33}\}6\%$
$\frac{3}{2}^-$	1637.8	1770	$\frac{3}{2}[512]63\% + \{\frac{7}{2}[514]Q_{22}\}8\%$
$\frac{3}{2}^+$		1785	$\{\frac{3}{2}[521]Q_{32}\}83\% + \{\frac{3}{2}[521]Q_{30}\}5\%$

[a]Energy of rotational band level (see Sec. IV).

well reproduced in our calculations (see Table IX). It should be noted that, in a more realistic picture, the spectroscopic factors with other main quantum numbers N and/or higher order nondiagonal effects stemming from quasiparticle-phonon admixtures to a state under consideration may modify the cross sections.

VII. CONCLUSIONS

In this work, the (n,γ), (d,p), and $(\mathbf{d},t)$ reactions measured with greatly improved resolution and sensitivity have been used to study the structure of the ^{159}Gd nucleus. A well established level scheme of this nucleus has been constructed confirming previous interpretation of levels lying below 1.2 MeV and introducing many changes and new levels namely above this energy. From our sets of extensive data, and including the results from primary γ rays from previous (n,γ) experiments, we have identified a total of 276 levels in ^{159}Gd.

The (n,γ) reaction was studied with high resolution bent-crystal spectrometers. We have observed 67 low-energy γ rays in ^{159}Gd; among these 35 γ rays are newly observed. Based on a precise fit of the highly accurate measured γ-ray transition energies and the proposed level energies, 59 of these transitions have been placed among low-lying levels.

In the (d,p) and $(\mathbf{d},t)$ reactions, about 200 levels with spin up to $\frac{11}{2}$ have been measured up to 2.3 MeV. Most of these levels are proposed with definite assignments of spins and parities thanks to the measurements done with a polarized deuteron beam. The DWBA formalism served as a useful tool to describe the differential cross sections of these reactions populating the vast majority of the levels reported. Several differential cross sections exhibited discrepancies with the DWBA predictions which may be due to higher order and multistep processes. A detailed description by the CCBA formalism is suggested as an attempt to describe these cases of anomalous angular dependencies of cross sections.

The interpretation of the structure of this nucleus has been provided for low-energy low-spin levels in terms of single quasiparticle excitations and their associated rotational bands. Essentially all levels below 800 keV have been identified. Several levels exhibiting large spectroscopic factors in the transfer reactions and lying between 800 keV and 1.8 MeV remain unidentified. In total, 68 experimentally observed levels have been grouped into rotational bands. We have confirmed or newly identify 12 negative parity bands and 9 positive parity bands. Tentative assignments for four of them have been suggested for the first time.

The intrinsic structure of levels was described within the quasiparticle-phonon model. Most of the experimentally observed low-lying levels ($E<1$ MeV) can be interpreted as members of rotational bands developed above states with

TABLE IX. Spectroscopic factors ($\times 10^{-3}$) of negative and positive parity bands in ^{159}Gd. Experimental values (from Table III) are compared with predictions of the Coriolis band mixing calulations. Only absolute values of the factors $S_{lj}(N=N_{\text{state}})$ with main quantum number of the dominant Nilsson assignment of a state are listed; quasiparticle-phonon admixtures are not taken into account. Also experimental level energies (in kilo-electron-volts) are compared with the model results.

				(d,p)		$(\mathbf{d},t)$[a]						(d,p)		$(\mathbf{d},t)$[a]	
State	I^π	E^{exp}	E^{th}	S_{lj}^{exp}	S_{lj}^{th}	S_{lj}^{exp}	S_{lj}^{th}	State	I^π	E^{exp}	E^{th}	S_{lj}^{exp}	S_{lj}^{th}	S_{lj}^{exp}	S_{lj}^{th}
$\frac{3}{2}^-[521]$	$\frac{3}{2}^-$	0.0	0	31	75	17	296	$\frac{5}{2}^+[642]$	$\frac{5}{2}^+$	67.829	74	1	2	0.5	24
	$\frac{5}{2}^-$	50.627	50	3	25	1.3	73		$\frac{7}{2}^+$	118.686	119		25	11	70
	$\frac{7}{2}^-$	121.899	121	59	149	23	860		$\frac{9}{2}^+$	185.0	184	64	105	9	417
	$\frac{9}{2}^-$	212.6	214	70	259	18	977		$\frac{11}{2}^+$	273.9	272	27	40	6	128
	$\frac{11}{2}^-$	324.9	325	24	12	3	223		$\frac{13}{2}^+$	372.7	368	149	352	54	1449
$\frac{5}{2}^-[523]$	$\frac{5}{2}^-$	146.316	146	27	86	6	101	$\frac{3}{2}^+[651]$	$\frac{3}{2}^+$	601.977	624	3	6	1.0	73
	$\frac{7}{2}^-$	227.412	227	78	252	8	506		$\frac{5}{2}^+$	646.697	621		14	0.5	239
	$\frac{9}{2}^-$	330.479	331	70	333	7	267		$\frac{7}{2}^+$	710.38	709.3		8		80
	$\frac{11}{2}^-$	456.4		41	108	4	280		$\frac{9}{2}^+$		789.7		1		49
$\frac{1}{2}^-[521]$	$\frac{1}{2}^-$	507.724	509	219	407	15	171	$\frac{7}{2}^+[633]$	$\frac{7}{2}^+$	633.60	625	7	18	0.6	38
	$\frac{3}{2}^-$	558.211	558	29	153	0.5	80		$\frac{9}{2}^+$		793		33		192
	$\frac{5}{2}^-$	588.517	589	67	255	10	179		$\frac{11}{2}^+$		800		19		78
	$\frac{7}{2}^-$	705.3	704	71	240	15	236		$\frac{13}{2}^+$	1093.0	1068	35	187		137
	$\frac{9}{2}^-$	759.8	759	74	188	21	206								
	$\frac{11}{2}^-$	938.7	939	15	67	9	108								
$\frac{11}{2}^-[505]$	$\frac{11}{2}^-$	684.16	684	17	98	82	1507								
$\frac{5}{2}^-[512]$	$\frac{5}{2}^-$	872.64	873		22		18	$\frac{3}{2}^+[402]$	$\frac{3}{2}^+$	744.378	745	31	115	230	1379
	$\frac{7}{2}^-$	948.35	948	462	419	6	131		$\frac{5}{2}^+$	800.45	800		16	6	237
	$\frac{9}{2}^-$	1043.2	1044	26	222	0.22	8		$\frac{7}{2}^+$	876.5	878	3	19	20	330
$\frac{3}{2}^-[532]$	$\frac{3}{2}^-$	1110.25	1116	6	5	49	24	$\frac{1}{2}^+[660]$	$\frac{1}{2}^+$	781.556	756	12	6	63	71
	$\frac{5}{2}^-$	1178.6	1176		41	9	628		$\frac{3}{2}^+$	858.51	868	2	4	7	63
	$\frac{7}{2}^-$	1239.4		1.9	16	16	763		$\frac{5}{2}^+$	818.89	835		7	2.5	146
	$\frac{9}{2}^-$	1365.9	1348		48	12	1238								
$\frac{1}{2}^-[530]$	$\frac{1}{2}^-$	1139.84	1142		9	85	70	$\frac{1}{2}^+[400]$	$\frac{1}{2}^+$	974.29	975	20	90	180	983
	$\frac{3}{2}^-$	1145.60	1158	4	34	154	476		$\frac{3}{2}^+$	1001.62	1000	3	49	43	783
	$\frac{5}{2}^-$	1253.1	1251		7	10	112		$\frac{5}{2}^+$	1059.6	1060	4	14	13	249
	$\frac{7}{2}^-$	1303.4		1.9	3	9	92		$\frac{7}{2}^+$	1120.3	1120		14	12	325
	$\frac{9}{2}^-$	1442.8	1455		10	19	42		$\frac{9}{2}^+$	1229.3	1229	13	3	7	77
$\frac{7}{2}^-[514]$	$\frac{7}{2}^-$	1134.7	1134	27	220	7	49	$\frac{7}{2}^+[404]$	$\frac{7}{2}^+$	1532.4	1486		47	6	1145
	$\frac{9}{2}^-$	1203.5	1204	66	329		43		$\frac{9}{2}^+$	1631.4	1574		4	2	99
$\frac{9}{2}^-[514]$	$\frac{9}{2}^-$		1517		7		78	$\frac{5}{2}^+[402]$	$\frac{5}{2}^+$	1964.6	1964		35	24	1130
	$\frac{11}{2}^-$	1622.3	1622		55	12	1440		$\frac{7}{2}^+$		2027		20		745
$\frac{1}{2}^-[510]$	$\frac{1}{2}^-$	1579.6	1606	8	9		3	$\frac{1}{2}^+[651]$	$\frac{1}{2}^+$	1983.3	1972	80	245		72
	$\frac{3}{2}^-$	1603.30	1599	93	30	6	6		$\frac{3}{2}^+$	2003.2	2027	7	215		89
	$\frac{5}{2}^-$	1693.5	1642	31	15		14		$\frac{5}{2}^+$	2088.1	2076	7	281		143
	$\frac{7}{2}^-$	1728.3	1668	1.9	76		110								
$\frac{3}{2}^-[512]$	$\frac{3}{2}^-$	1637.8	1674	22	21	2.0	4								
	$\frac{5}{2}^-$	1702.1	1754	16	13	2.6	8								
	$\frac{7}{2}^-$	1809.2	1825	10	32		93								
$\frac{1}{2}^-[770]$	$\frac{1}{2}^-$		1925		8		1								
	$\frac{3}{2}^-$	1997.3	1997	28	69		6								

TABLE IX. (*Continued.*)

State	I^π	E^{exp}	E^{th}	(d,p) S_{lj}^{exp}	(d,p) S_{lj}^{th}	$(\mathbf{d},t)^{a}$ S_{lj}^{exp}	$(\mathbf{d},t)^{a}$ S_{lj}^{th}	State	I^π	E^{exp}	E^{th}	(d,p) S_{lj}^{exp}	(d,p) S_{lj}^{th}	$(\mathbf{d},t)^{a}$ S_{lj}^{exp}	$(\mathbf{d},t)^{a}$ S_{lj}^{th}
	$\frac{5}{2}^-$		2177		37		4								
	$\frac{7}{2}^-$	2058.0	2056	33	36		4								

[a]Experimental values below 650 keV are deduced from one angle measurement. $S_{lj}^{\mathrm{exp}}=(G_{lj}/2j+1)$.

significant quasiparticle components ($>70\%$). However, several high-lying states should be understood as complex combinations of single quasiparticle and quasiparticle-vibrational states. States calculated with dominant vibrational components are suggested, preferentially above 1.8 MeV. Rotational bands were modelled in the quasiparticle-rotor approach. Coriolis band mixing calculations revealed that several experimentally observed rotational bands should be considered as bands built upon mixed Nilsson configurations. The spectroscopic factors calculated in our model for the pickup and stripping reactions reasonably agree with the experimental data for the levels interpreted.

ACKNOWLEDGMENTS

This work has been carried out in frame of the research program No. MSM 210 000 018 of the Ministry of Education, Youth and Sport of the Czech Republic. The support of the Czech Committe for Cooperation with JINR Dubna, the ILL Grenoble, the TU-Munich and the Deutsche Forschungsgemeinschaft are gratefully acknowledged. One of the authors (D.N.) thanks the Ministry of Education, Youth and Sport of the Czech Republic for support under Contract No. LNA00A006. The authors thank Ivo Tomandl from the NPI at Řež for the discussions on DWBA and Michael Jentschel of the ILL Grenoble for the measurement of the 507.668 keV doublet with the double-flat-crystal GAMS4 spectrometer.

[1] P. O. Tjøm and B. Elbek, K. Dan. Vidensk. Selsk. Mat. Fys. Medd. **36**, 8 (1967).
[2] M. Jaskóla, K. Nybø, P. O. Tjøm, and B. Elbek, Nucl. Phys. A **96**, 52 (1968).
[3] J. C. Peng, J. V. Maher, G. H. Wedberg, and C. M. Cheng, Phys. Rev. C **13**, 1451 (1976).
[4] G. Løvhøiden, T. F. Thorsteinsen, E. Andersen, M. F. Kiziltan, and D. G. Burke, Nucl. Phys. A **494**, 157 (1989).
[5] M. Jaskóla, J. Turkiewicz, L. Zemlo, and W. Osakiewicz, Acta Phys. Pol. B **2**, 521 (1971).
[6] L. Glowacka, M. Jaskóla, M. Kozlowski, J. Turkiewicz, L. Zemlo, and W. Osakiewicz, Polish Inst. Nucl. Res. Rep. /I/ PL/A 1468(1973).
[7] L. V. Groshev, A. M. Demidov, and L. L. Sokolovskii, Bull. Acad. Sci. USSR, Phys. Ser. (Engl. Transl.) **1947**, 1644 (1971).
[8] R. C. Greenwood and R. E. Chrien, Bull. Am. Phys. Soc. **22**, 1032 (1977).
[9] R. G. Helmer, Nucl. Data Sheets **72**, 83 (1994).
[10] P. Kemnitz, L. Funke, K. H. Kaun, H. Sodan, and G. Winter, Nucl. Phys. A **137**, 679 (1969).
[11] C. Granja, S. Pospíšil, J. Kubašta, and S. A. Telezhnikov, Nucl. Phys. A **724**, 14 (2003).
[12] C. Granja, S. Pospíšil, R. E. Chrien, and S. A. Telezhnikov, Nucl. Phys. A **729**, 679 (2003).
[13] S. Pospíšil, F. Bečvář, C. Granja, and S. A. Telezhnikov, J. Res. Natl. Inst. Stand. Technol. **105**, 173 (2000).
[14] H. H. Schmidt, T. von Egidy, H. J. Scheerer, P. Hungerford, H. G. Börner, S. A. Kerr, K. Schreckenbach, R. F. Casten, W. R. Kane, D. D. Warner, *et al.*, Nucl. Phys. A **454**, 267 (1986).
[15] H. H. Schmidt, W. Stöffl, T. von Egidy, P. Hungerford, K. Schreckenbach, H. G. Börner, D. D. Warner, R. E. Chrien, R. C. Greenwood, and C. W. Reich, J. Phys. G **12**, 411 (1986).
[16] V. A. Bondarenko, A. V. Afanasjev, F. Bečvář, J. Honzátko, M. E. Montero-Cabrera, I. Kuvaga, S. J. Robinson, A. M. J. Spits, and S. A. Telezhnikov, Nucl. Phys. A **726**, 175 (2003).
[17] M. E. Bunker and C. W. Reich, Rev. Mod. Phys. **43**, 348 (1971).
[18] A. K. Jain, R. K. Sheline, and P. C. Sood, Rev. Mod. Phys. **62**, 393 (1990).
[19] B. Hird and K. H. Huang, Can. J. Phys. **53**, 559 (1975).
[20] I. Kanestrøm and P. O. Tjøm, Nucl. Phys. A **164**, 664 (1971).
[21] B. L. Andersen, B. B. Back, and J. M. Bang, Nucl. Phys. A **147**, 33 (1970).
[22] J. V. Maher, G. H. Wedberg, J. J. Kolata, J. C. Peng, and J. L. Ricci, Phys. Rev. C **8**, 2390 (1973).
[23] J. C. Peng, H. S. Song, F. C. Wang, and J. V. Maher, Phys. Rev. Lett. **41**, 225 (1978).
[24] J. C. Peng, H. S. Song, F. C. Wang, and J. V. Waher, Nucl. Phys. A **341**, 440 (1980).
[25] C. Vargas, J. G. Hirsh, T. Beuschel, and J. P. Draayer, Phys. Rev. C **61**, 031301 (2000).
[26] C. Vargas, J. G. Hirsh, and J. P. Draayer, Nucl. Phys. A **673**, 219 (2000).
[27] C. Vargas, J. G. Hirsh, and J. P. Draayer, Los Alamos X-preprint No. 0208062 (2002).
[28] F. A. Gareev, S. P. Ivanova, V. G. Soloviev, and S. I. Fedotov, Sov. J. Part. Nucl. **4**, 148 (1973).
[29] V. G. Soloviev, *Theory of Atomic Nuclei: Quasiparticles and Phonons* (Institute of Physics, Philadelphia, 1992).
[30] H. R. Koch, H. G. Börner, J. A. Pinston, W. F. Davidson, J. Fadou, R. Roussille, and O. W. B. Schultz, Nucl. Instrum.

Methods **175**, 401 (1980).
[31] S. F. Mughabghab, M. Divadeenam, and N. E. Holden, *BNL-325 Tables, Part B 1* (Academic Press, New York, 1981).
[32] H. R. Koch, Kernforschungsanlage Jülich GmbH **10**, 1 (1978).
[33] J. Klora, H. G. Börner, T. von Egidy, R. Georgii, J. Jolie, S. Judge, V. A. Khitrov, B. Krushe, V. A. Libman, H. Lindner, *et al.*, Nucl. Phys. A **561**, 1 (1993).
[34] H. G. Börner, J. Jolie, F. Hoyler, S. J. Robinson, M. S. Dewey, G. Greene, E. G. Kessler, and R. D. Deslattes, Phys. Lett. B **215**, 45 (1988).
[35] F. Rieß, Annual Report, Beschleunigerlaboratorium, Universität und Technische Univesität Müchen, 1991.
[36] R. W. Hoff, W. F. Davidson, D. D. Warner, H. G. Börner, and T. von Egidy, Phys. Rev. C **25**, 2232 (1982).
[37] H. H. Schmidt, P. Hungerford, H. Daniel, T. von Egidy, S. A. Kerr, R. Brissot, G. Barreau, H. G. Börner, C. Hofmeyr, and K. P. Lieb, Phys. Rev. C **25**, 2888 (1982).
[38] W. Assmann *et al.*, Nucl. Instrum. Methods **122**, 191 (1974).
[39] M. Löffler, H. J. Scheerer, and H. Vonach, Nucl. Instrum. Methods **111**, 1 (1973).
[40] E. Zanotti, M. Bisenberger, R. Hertenberger, H. Kader, and G. Graw, Nucl. Instrum. Methods Phys. Res. A **310**, 706 (1991).
[41] C. Granja, Ph.D. thesis, Czech Tech. Univ. in Prague, http://kf-alpha.fjfi.cvut.cz/~granja/phd/thesis.html, 2003.
[42] A. Metz, Diploma thesis, L. M. Univ. München, 1999.
[43] H. F. Wirth, H. Angerer, T. von Egidy, Y. Eisermann, G. Graw, and R. Hertenberger, Annual Report, Beschleunigerlaboratorium, Universität und Technische Universität München, 2000.
[44] H.-F. Wirth, Ph.D. thesis, Tech. Univ. München, http://tumb1.biblio.tumuenchen.de/publ/diss/ph/2001/wirth.html, 2001.
[45] R. Hertenberger, Y. Eisermann, H.-F. Wirth, and G. Graw, Annual Report, Beschleunigerlaboratorium, Universität und Technische Universität München, 2000.
[46] P. D. Kunz, CHUCK3 Code, University of Colorado, 1980.
[47] W. W. Daehnick, J. D. Childs, and Z. Vrcelej, Phys. Rev. C **21**, 2253 (1980).
[48] F. D. Bechetti and G. W. Greenless, Phys. Rev. **182**, 1190 (1968).
[49] R. P. Ward and P. R. Hayes, At. Data Nucl. Data Tables **49**, 315 (1991).
[50] R. B. Firestone and V. S. Shriley, *Table of Isotopes* (J. Wiley, New York, 1996).
[51] K. Schreckenbach, LeFit Code, TU-München, 1985.
[52] R. G. Helmer, Nucl. Data Sheets **83**, 285 (1998).
[53] C. W. Reich, Nucl. Data Sheets **71**, 709 (1994).
[54] R. G. Helmer, Nucl. Data Sheets **78**, 219 (1996).
[55] C. W. Reich and R. G. Helmer, Nucl. Data Sheets **90**, 645 (2000).
[56] B. Singh, Nucl. Data Sheets **89**, 1 (2000).
[57] S. G. Nilsson, Mat. Fys. Medd. K. Dan. Vidensk. Selsk. **29**, 16 (1955).
[58] B. E. Chi, Nucl. Phys. **83**, 97 (1966).
[59] V. A. Bondarenko and M. Jaskóla (private communication, 2002).
[60] D. Nosek, R. K. Sheline, P. C. Sood, and J. Kvasil, Int. J. Mod. Phys. E **1**, 793 (1992).
[61] L. K. Peker, Nucl. Data Sheets **65**, 439 (1992).